Since January 2020 Elsevier has created a COVID-19 resource centre with free information in English and Mandarin on the novel coronavirus COVID-19. The COVID-19 resource centre is hosted on Elsevier Connect, the company's public news and information website.

Cell

SARS-CoV-2 mRNA vaccination elicits a robust and persistent T follicular helper cell response in humans

Graphical abstract

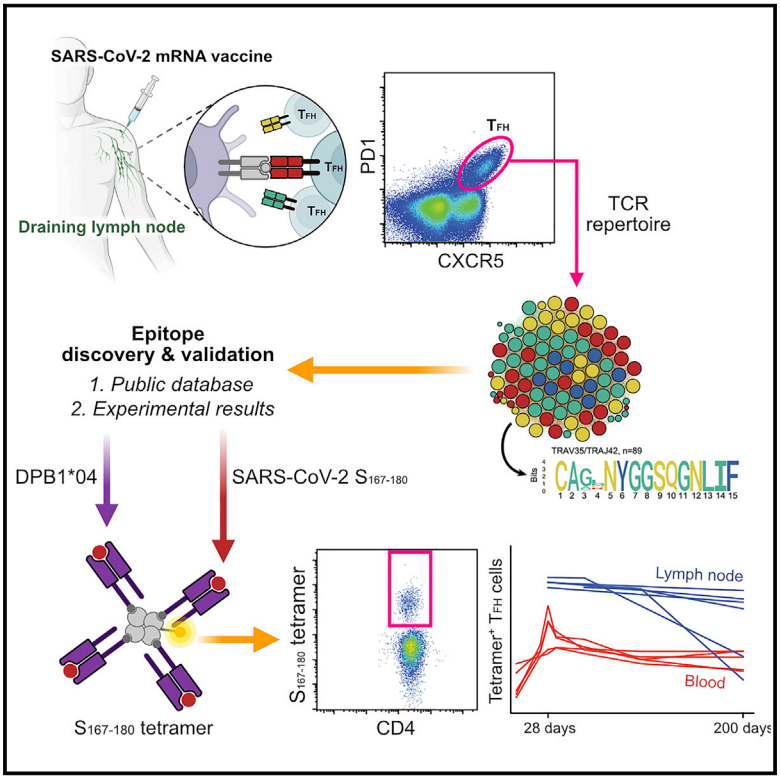

Authors

Philip A. Mudd, Anastasia A. Minervina, Mikhail V. Pogorelyy, ..., Jamie Rossjohn, Paul G. Thomas, Ali H. Ellebedy

Correspondence

pmudd@wustl.edu (P.A.M.), paul.thomas@stjude.org (P.G.T.), ellebedy@wustl.edu (A.H.E.)

In brief

Analysis of draining lymph nodes of individuals vaccinated with BNT162b2 mRNA vaccine against SARS-CoV-2 identifies viral-spike-specific follicular helper CD4$^+$ T cells that persist for months and contribute to long-term immunity.

Highlights

- SARS-CoV-2 vaccines induce robust human T_{FH} cell responses in draining lymph nodes
- HLA-DPB1*04 restricts the immunodominant SARS-CoV-2 $S_{167–180}$ epitope
- $S_{167–180}$ is recognized by T cell receptors with a public α-chain motif
- S-specific T_{FH} cells are maintained in draining lymph nodes 6 months after vaccination

Mudd et al., 2022, Cell *185*, 603–613
February 17, 2022
https://doi.org/10.1016/j.cell.2021.12.026

Cell

CellPress

Article

SARS-CoV-2 mRNA vaccination elicits a robust and persistent T follicular helper cell response in humans

Philip A. Mudd,[1,2,16,*] Anastasia A. Minervina,[3,16] Mikhail V. Pogorelyy,[3,16] Jackson S. Turner,[4] Wooseob Kim,[4] Elizaveta Kalaidina,[5] Jan Petersen,[6] Aaron J. Schmitz,[4] Tingting Lei,[4] Alem Haile,[7] Allison M. Kirk,[3] Robert C. Mettelman,[3] Jeremy Chase Crawford,[3] Thi H.O. Nguyen,[8] Louise C. Rowntree,[8] Elisa Rosati,[9] Katherine A. Richards,[10] Andrea J. Sant,[10] Michael K. Klebert,[7] Teresa Suessen,[11] William D. Middleton,[11] SJTRC Study Team, Joshua Wolf,[12] Sharlene A. Teefey,[11] Jane A. O'Halloran,[13] Rachel M. Presti,[2,7,13,15] Katherine Kedzierska,[8] Jamie Rossjohn,[6,14] Paul G. Thomas,[3,*] and Ali H. Ellebedy[2,4,15,17,*]

[1]Department of Emergency Medicine, Washington University School of Medicine, Saint Louis, MO 63110, USA
[2]Center for Vaccines and Immunity to Microbial Pathogens, Washington University School of Medicine, Saint Louis, MO 63110, USA
[3]Department of Immunology, St. Jude Children's Research Hospital, Memphis, TN 38105, USA
[4]Department of Pathology and Immunology, Washington University School of Medicine, Saint Louis, MO 63110, USA
[5]Division of Allergy and Immunology, Department of Internal Medicine, Washington University School of Medicine, Saint Louis, MO 63110, USA
[6]Infection and Immunity Program & Department of Biochemistry and Molecular Biology, Biomedicine Discovery Institute, Monash University, Clayton, Victoria 3800, Australia
[7]Clinical Trials Unit, Washington University School of Medicine, Saint Louis, MO 63110, USA
[8]Department of Microbiology and Immunology, University of Melbourne, at Peter Doherty Institute for Infection and Immunity, Parkville, Victoria 3052, Australia
[9]Institute of Clinical Molecular Biology, Christian-Albrecht University of Kiel, Kiel 24105, Germany
[10]David H. Smith Center for Vaccine Biology and Immunology, Department of Microbiology and Immunology, University of Rochester Medical Center, Rochester, NY 14642, USA
[11]Mallinckrodt Institute of Radiology, Washington University School of Medicine, Saint Louis, MO 63110, USA
[12]Department of Infectious Diseases, St. Jude Children's Research Hospital, Memphis, TN 38105, USA
[13]Division of Infectious Diseases, Department of Internal Medicine, Washington University School of Medicine, Saint Louis, MO 63110, USA
[14]Institute of Infection and Immunity, Cardiff University, School of Medicine, Heath Park, Cardiff CF14 4XN, UK
[15]Andrew M. and Jane M. Bursky Center for Human Immunology and Immunotherapy Programs, Washington University School of Medicine, Saint Louis, MO 63110, USA
[16]These authors contributed equally
[17]Lead contact
*Correspondence: pmudd@wustl.edu (P.A.M.), paul.thomas@stjude.org (P.G.T.), ellebedy@wustl.edu (A.H.E.)
https://doi.org/10.1016/j.cell.2021.12.026

SUMMARY

SARS-CoV-2 mRNA vaccines induce robust anti-spike (S) antibody and $CD4^+$ T cell responses. It is not yet clear whether vaccine-induced follicular helper $CD4^+$ T (T_{FH}) cell responses contribute to this outstanding immunogenicity. Using fine-needle aspiration of draining axillary lymph nodes from individuals who received the BNT162b2 mRNA vaccine, we evaluated the T cell receptor sequences and phenotype of lymph node T_{FH}. Mining of the responding T_{FH} T cell receptor repertoire revealed a strikingly immunodominant HLA-DPB1*04-restricted response to $S_{167–180}$ in individuals with this allele, which is among the most common HLA alleles in humans. Paired blood and lymph node specimens show that while circulating S-specific T_{FH} cells peak one week after the second immunization, S-specific T_{FH} persist at nearly constant frequencies for at least six months. Collectively, our results underscore the key role that robust T_{FH} cell responses play in establishing long-term immunity by this efficacious human vaccine.

INTRODUCTION

The COVID-19 pandemic necessitated rapid late-stage clinical trials of mRNA vaccine technology (Anderson et al., 2020; Baden et al., 2021; Jackson et al., 2020; Polack et al., 2020; Verbeke et al., 2021; Walsh et al., 2020; Widge et al., 2021) that resulted in the first FDA-approved vaccine using this technology platform. The two mRNA vaccines developed by Pfizer/BioNTech (BNT162b2) (Polack et al., 2020) and Moderna (mRNA-1273) (Baden et al., 2021) have proven instrumental in the initiation of widespread vaccination campaigns in the United States and around the world. Both vaccines engender high-titer circulating

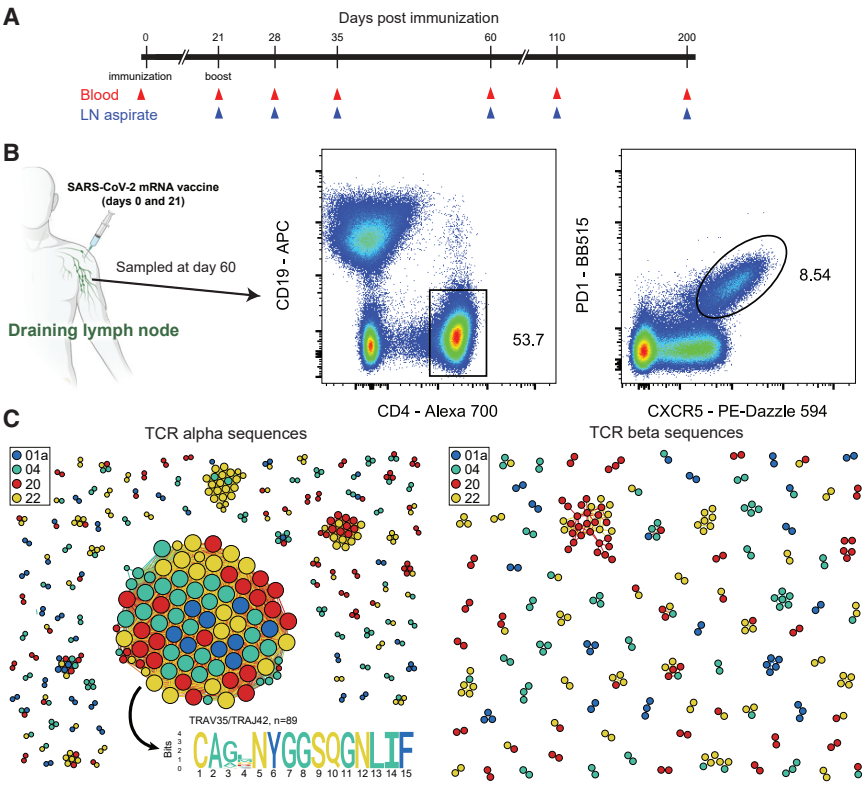

Figure 1. T cell receptor sequences from sorted human lymph node T_{FH} cells following mRNA vaccination

(A) Study timeline. Day 0 blood samples were obtained prior to the first dose of the vaccine and day 21 samples were taken prior to the second dose of the vaccine.

(B) Sorting strategy for T_{FH} cells from LN aspiration samples obtained on day 60.

(C) Similarity network of the 500 most abundant TCRα sequences (left) and TCRβ sequences (right) from the lymph node TCR repertoire obtained from sorted T_{FH} cells of 4 individual donors (01a, 04, 20, and 22) 60 days after mRNA vaccination. Each vertex corresponds to an individual TCR clonotype, which are connected to adjacent data points if they have identical VJ-segments and less than 2 mismatches in the CDR3 amino acid sequence. The size of the vertex corresponds to the vertex degree (number of neighbors).

anti-SARS-CoV-2 spike-protein-specific antibodies that can neutralize the originally circulating SARS-CoV-2 strain (Jackson et al., 2020; Walsh et al., 2020) as well as other variants that have emerged since the vaccine design phase (Chen et al., 2021; Wang et al., 2021a, 2021b; Wu et al., 2021). Neutralizing antibodies induced by mRNA vaccines appear to be the key correlate of protection from COVID-19 in animal models (Corbett et al., 2021) and in humans (Khoury et al., 2021). COVID-19 mRNA vaccines exhibit the highest efficacy in phase 3 studies among widely utilized COVID-19 vaccines worldwide (Al Kaabi et al., 2021; Baden et al., 2021; Logunov et al., 2021; Polack et al., 2020; Sadoff et al., 2021; Voysey et al., 2021). Understanding exactly how mRNA vaccines elicit such robust and protective immune responses in humans is necessary for extending the application of this novel platform to vaccines against other important human pathogens.

Germinal center (GC) reactions that occur in draining lymph nodes following infection or vaccination are critical for developing long-lasting, high-affinity antibody responses (Ripperger and Bhattacharya, 2021; Victora and Nussenzweig, 2012). T follicular helper (T_{FH}) cell responses in the lymph node are necessary for forming and sustaining GC reactions and for the development of both long-lived plasma cells and memory B cells (Crotty, 2011; Qi, 2016; Ueno et al., 2015). Detailed analysis of the specificity and dynamics of vaccination-induced GC reactions in humans is increasingly being explored through sampling draining lymph nodes using serial fine-needle aspiration (FNA) following intramuscular immunization (Turner et al., 2020, 2021; Kim et al., 2021). Importantly, it appears that the GC reaction in humans persists over a longer period (Turner et al., 2020, 2021; Kim et al., 2021) than what was anticipated from studies in preclinical animal models (Good-Jacobson et al., 2014; Weisel et al., 2016). Determining the epitope targets and dynamics of SARS-CoV-2-specific T_{FH} cells induced in human draining lymph nodes during an active immune response is critical to understanding the role of T_{FH} cells in the development of long-lived plasma cells and memory B cells following vaccination.

RESULTS

Human T_{FH} population size mirrors the GC B cell population following mRNA vaccination

We conducted a prospective observational study to follow vaccine-induced immune responses in a cohort of 41 healthy adults who had received the BNT162b2 mRNA vaccine (Turner et al., 2021). Demographics of the full cohort have previously been reported (Turner et al., 2021). Fifteen members of the cohort underwent axillary lymph node FNA. All subjects were vaccinated with two 30 μg doses of BNT162b2, approximately twenty-one days apart. Blood and/or FNA samples were obtained at day 0 (prior to the first vaccine dose), day 21 (immediately prior to the second vaccine dose), day 28, day 35, day 60, day 110, and day 200 according to the schedule listed in Figure 1A. This manuscript reports exclusively on the 15 subjects who underwent lymph node FNA. Demographics of the included individuals are listed in Table 1. None of the included subjects reported previous infection with SARS-CoV-2.

We first evaluated the size of the human T_{FH} population in relation to the size of the GC B cell population in the lymph node. We analyzed the frequency of the GC B cell response (defined as $CD19^{+}IgD^{low}Bcl\text{-}6^{+}CD38^{int}$ B cells) among all lymph-node-resident B cells and the frequency of total lymph-node-resident

Table 1. Cohort demographics

Study ID	Sex	Race	Ethnicity	Age	Number of lymph nodes sampled
01a	Male	White	Non-hispanic	34	1
02a	Male	White	Hispanic	37	2
04	Female	White	Non-hispanic	38	2
07	Female	White	Non-hispanic	33	1
08	Female	White	Non-hispanic	27	1
10	Female	White	Non-hispanic	27	2
13	Male	White	Non-hispanic	34	1
15	Female	Black	Non-hispanic	52	2
16	Male	White	Non-hispanic	37	2
20	Female	White	Non-hispanic	48	2
21	Female	White	Non-hispanic	31	1
22	Male	White	Non-hispanic	36	1
26	Female	White	Non-hispanic	38	1
28	Female	Asian	Non-hispanic	44	1
43	Male	Asian	Non-hispanic	40	1

$CD4^+$ T cells that exhibited a T_{FH} cell phenotype ($Bcl\text{-}6^+CXCR5^+PD1^+FoxP3^-$) in 95 separate lymph node samples taken from each of the 15 individuals over the course of the study (Figure S1A; Table S1). These FNA samples were obtained between 21 and 200 days following primary vaccination. Six of the fifteen subjects underwent repeated sampling of two separate axillary lymph nodes (Table S1). We found a significant correlation between the size of the GC B cell population in the lymph node and the total T_{FH} cell population frequency following mRNA vaccination (Figure S1B). We also noted a significant correlation between the size of the SARS-CoV-2 spike-specific GC B cell population in the lymph node and the total lymph node T_{FH} cell population frequency (Figure S1C).

Discovery and characterization of an immunodominant DPB1*04:01-restricted $CD4^+$ T cell population

Next, we sought to illuminate the antigen specificity of the lymph node T_{FH} population. To do this, we sorted total T_{FH} cells from FNA samples obtained on day 60 from four separate subjects (Figure 1B) and reconstructed their T cell receptor (TCR) repertoires using unpaired sequencing of the TCRα and TCRβ chains (Figure 1C). Surprisingly, clonally expanded TCRs formed a prominent α-chain cluster that was shared among all 4 donors (Figure 1C), corresponding to 0.9%–7.7% of the total lymph node T_{FH} cells in each donor. We did not observe a similar shared cluster in the TCRβ chain repertoires. We observed the same α-motif in a previously published paper (Minervina et al., 2021a), where it was the largest signal and corresponded to 0.2% of total $CD4^+$ T cells and 16.3% of estimated SARS-CoV-2-responding $CD4^+$ T cells in the blood at the peak of the acute response. Large clusters of TCRs with sequence similarity are an indication of convergent selection of similar receptors to the same antigen (Dash et al., 2017; Glanville et al., 2017; Pogorelyy et al., 2019). As this motif was present among expanded clones in many donors, it likely recognizes an immunodominant epitope from SARS-CoV-2 presented in the context of a common HLA class II allele.

In order to decode the specificity of the heterodimer $\alpha\beta$TCR, we first needed to determine what β-chains pair with the TCRα chain motif that we identified (Figure 2A). To do this, we queried publicly available $CD4^+$ paired TCR datasets. We used two datasets that have paired $\alpha\beta$TCR sequences from $CD4^+$ T cells after antigen-reactive T cell enrichment following stimulation with SARS-CoV-2 peptides (Bacher et al., 2020; Meckiff et al., 2020). We searched for our CDR3α motif ("CA[G/A/V]XNYGGSQGNLIF") in these datasets and found 1,329 out of 44,256 unique TCRs in Bacher et al., but only 53 out of 43,745 in Meckiff et al. with the matched CDR3α motif. Next, we used the identified β chains to look for overlap in the MIRA dataset (Nolan et al., 2020)—a large dataset produced by Adaptive Biotech linking TCR sequences to SARS-CoV-2 epitopes. We identified 64 TCRs from Bacher et al. highly similar (up to one amino acid mismatch in CDR3, identical CDR1 and CDR2) to MIRA TCRs reactive to the overlapping peptide pool from SARS-CoV-2 spike (S) protein 160–218 positions (Figure 2B). Interestingly, this part of the S protein was not used for stimulation in Meckiff et al., explaining why we found only a small number of TCRs of interest in this dataset and indirectly supporting the predicted identification of the peptide region from the MIRA dataset.

Five of six subjects recognizing this peptide pool in the MIRA database had available HLA-typing. These five shared the DPB1*04:(01/02) and DQB1*06:(02/03) alleles. To establish HLA restriction of the response of interest and to narrow the search to a single peptide, we used NetMHCII2.3 (Jensen et al., 2018) to look for predicted epitopes from the $S_{160–218}$ peptide pool that are presented by one or both of these shared alleles. We found that peptides containing the core sequence YVSQPFLMD were predicted to strongly bind the DPB1*04:01 and DPB1*04:02 alleles, while no strong binders were identified for the DQB1*06:(02/03) alleles. Interestingly, SARS-CoV-2 epitopes with this core sequence (YVSQPFLMD, $S_{170–178}$) have previously been described in prominent epitope discovery studies

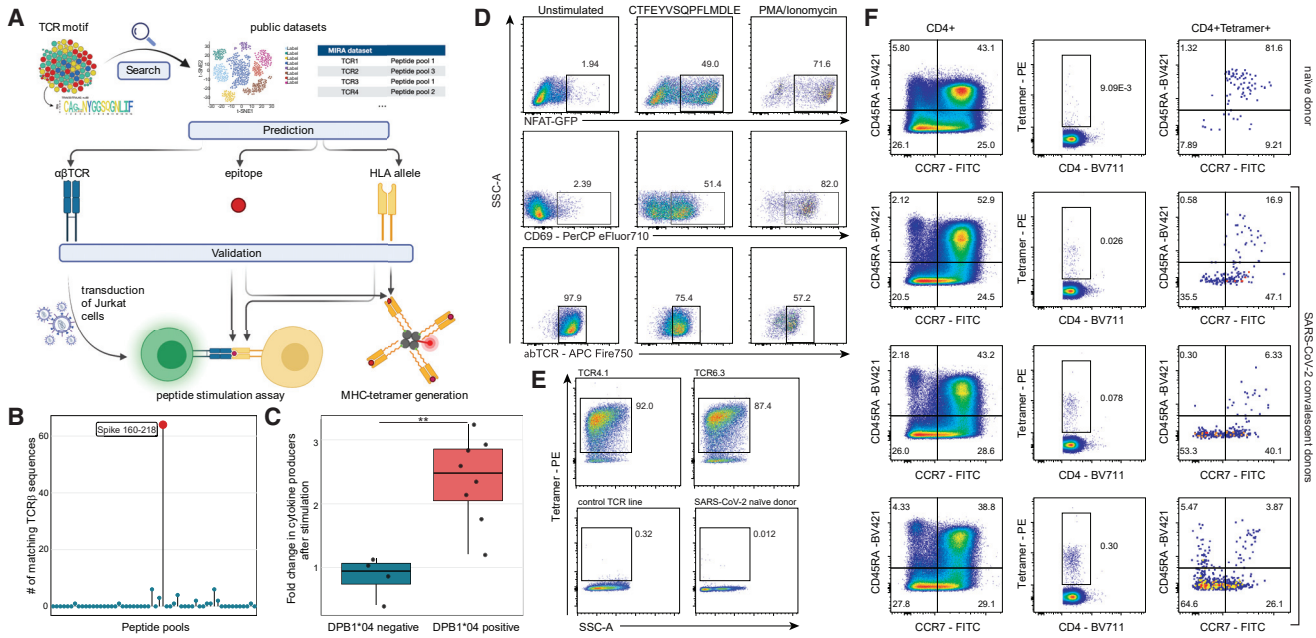

Figure 2. $S_{167–180}$ epitope discovery and HLA class II tetramer validation

(A) Response identification process. The identified TCRα motif of interest was used to query large public scRNA-seq datasets (Bacher et al., 2020; Meckiff et al., 2020) to identify potential partner TCRβ chains and then matched to the large MIRA dataset that used TCRβ sequencing (Nolan et al., 2020) to predict HLA-restriction and cognate epitopes. To validate our prediction, we generated a T cell line expressing the putative αβTCR and we generated HLA class II tetramers.

(B) Identification of peptide pool for the motif TCRs using the MIRA dataset. TCRβ chains from paired αβTCRs with CDR3α motif (CA[G/A/V]XNYGGSQGNLIF) were searched in the MIRA dataset allowing for up to one mismatch in CDR3 amino acid sequence. The y axis shows the number of TCRβ chains from Bacher et al. matching to TCRβ from different MIRA SARS-CoV-2 peptide pools. Largest hit (red dot) corresponded to the peptide pool spanning amino acid positions 160–218 from S protein.

(C) Average fold change in $CD4^+/CD69^+$ T cells (producing IL2, TNFα, or IFNγ) per 10^6 cells following CTFEYVSQPFLMDLE peptide stimulation of DPB1*04-positive and -negative SJTRC PBMCs. PBMCs collected during SARS-CoV-2 convalescence or post-vaccination with BNT162b2 were used for intracellular cytokine staining assay. Average fold changes were compared using a Mann-Whitney U test; p = 0.004. Gating strategy is shown in Figure S2.

(D) Jurkat cell line expressing the predicted TCR after stimulation with the predicted epitope. Left column: negative control; middle column: TCR4.1 cell line co-cultured with PBMCs from healthy DPB1*04:01-positive donor pulsed with CTFEYVSQPFLMDLE peptide ($S_{167–180}$); right column: positive control. Top row: NFAT-GFP reporter expression. Middle row: CD69 surface expression. Bottom row: downregulation of the TCR on cell surface.

(E) $S_{167–180}$ tetramer staining identifies epitope-specific T cells with high specificity. Top row: staining of TCR4.1 and TCR6.3 Jurkat cell lines. Bottom left: staining of Jurkat cell line expressing TCR with other known specificity; bottom right: staining of PBMCs from SARS-CoV-2-naive individual.

(F) $S_{167–180}$ $tetramer^+$ cells have predominantly effector memory phenotype in SARS-CoV-2-convalescent patients. Each row represents an individual donor. Left column: CCR7 and CD45RA distribution in bulk $CD3^+CD4^+$ cells. Middle column: $S_{167–180}$ tetramer staining of $CD3^+CD4^+$ cells. Right column: memory/naive phenotypes of $CD3^+CD4^+S_{167–180}$ $tetramer^+$ cells. Gating strategies for (D), (E), and (F) are shown in Figure S3.

(Peng et al., 2020; Tarke et al., 2021), in which the response was identified in multiple donors. However, this response has not previously been reported to be HLA-DPB1*04-restricted.

As an initial investigation of this possible HLA restriction, we obtained post-vaccination peripheral blood from participants in the ongoing SJTRC study (SJTRC, NCT04362995). PBMCs from these participants were stimulated with purified $S_{166–180}$ peptide (CTFEYVSQPFLMDLE) and the responses were measured by intracellular cytokine staining and flow cytometry. We determined that participants with the HLA-DPB1*04 allele had increased cell counts per million PBMCs of monofunctional $CD4^+CD69^+$ T cells producing IL-2, TNFα, or IFNγ compared with participants without this allele (Figures 2C, S2B, and S2C). Further, we noted that each DPB1*04^+ donor had activated poly-functional T cells producing two or three cytokines in response to peptide stimulation, in both vaccinated-naive and SARS-CoV-2-convalescent individuals (Figures S2D and S2E).

We then moved forward with more rigorous experimental validation of our paired TCR, peptide epitope, and restricting HLA combination (Figure 2A). To do this, we selected two paired TCRs from Bacher et al. that included the same TCRα but distinct TCRβ chains that we designated TCR4.1 and TCR6.3. We transduced these each into separate Jurkat TCR-negative cell lines that also express an endogenous NFAT-GFP reporter to allow for tracking of intracellular signaling downstream of the transduced paired TCR following TCR engagement. The TCR-transduced Jurkat cell lines were co-cultured with PBMCs from an HLA-DPB1*04^+ donor and pulsed with $S_{166–180}$ peptide to evaluate TCR activation. Consistent with our prediction, we observed strong NFAT activation from the CTFEYVSQPFLMDLE-stimulated cells expressing either TCR pairing (Figures 2D, S3, and S4). Further, we performed additional stimulation experiments employing a mutant version of the $S_{166–180}$ peptide found in the GISAID database (CTFEYSQPFFMDLE) as well as

a set of overlapping peptides (Figure S4) to determine the core peptide required for TCR engagement. Both TCR lines recognized the mutated epitope as well as the overlapping peptides containing the YVSQPFLM amino acid stretch, suggesting that this core sequence is crucial to TCR engagement. Interestingly, this core is truncated at P8 in comparison to the core predicted by NetMHC (YVSQPFLMD). In contrast, the N-terminal portion of the core (YVSQPFLMD) did not tolerate any truncations, highlighting the importance of P1 and providing a clear specificity control for the peptide stimulation experiment. In a canonical orientation of the TCR binding to HLA-DPB1*04, the TCRα chain can be expected to reside above the N-terminal portion of the peptide, whereas the β-chain should reside above the C-terminal portion of the peptide. It is reasonable to assume that preferential TRAV35 selection is driven by some strong interactions between the TCRα chain and a feature in the N-terminal portion of the peptide. Thus, a TRAV-biased TCR may be particularly sensitive to a truncation of the peptide N terminus. The selection of multiple TRBV gene segments suggests that interactions between peptide and TCRβ chain are less critical, which may explain why the P8 truncation is tolerated.

Next, we generated an HLA class II tetramer to probe the antigen-specific T cell response that we had discovered. We tested our HLA-DPB1*04 $S_{167–180}$ tetramer using the two transduced TCR4.1 and TCR6.3 Jurkat cell lines and showed high sensitivity and low background staining (Figure 2E). We then used the $S_{167–180}$ tetramer to look for antigen-specific $CD4^+$ T cells in PBMC from three HLA-DPB1*04^+ SARS-CoV-2-convalescent donors and a control HLA-DPB1*04^+ SARS-CoV-2-naive donor. We found a small number of tetramer-specific cells predominantly in the naive subpopulation ($CCR7^+CD45RA^+$) in the naive donor and a much larger number of tetramer-specific cells that were primarily effector memory ($CCR7^-CD45RA^-$) in the SARS-CoV-2-convalescent donors (Figure 2F). The frequency of tetramer-positive cells was comparable to the frequencies of the total S-specific cells observed using a separate activation-induced marker (AIM) assay with overlapping S-peptides (Figure S5), suggesting that tetramer staining provided a higher sensitivity to detect epitope-specific responses. We then sequenced tetramer-specific TCRs from these convalescent donors using our previously described scTCR-seq approach (Wang et al., 2012). The majority (64%) of sequenced cells had the same TRAV35-CA[G/A/V]XNYGGSQGNLIF TCRα motif that we had initially identified, and >80% of all sequences included TRAV35, suggesting that the discovered TCRα motif is the most frequent mode of recognition for this epitope (Table S2). We also found the TCR4.1β (exactly matching amino acid sequence) and TCR6.3β (one mismatch) in the single-cell TCR sequencing of tetramer-specific T cells from convalescent individuals. This is a further independent validation that the αβTCRs selected for Jurkat cell line generation are $S_{167–180}$ specific and occur in multiple patients.

Tracking $S_{167–180}$ antigen-specific $CD4^+$ T cell responses in blood and draining lymph nodes following BNT162b2 vaccination

With the discovery of an immunodominant SARS-CoV-2-S epitope restricted by the HLA-DPB1*04:01 allele that is found at high frequency (>40%) in many populations around the world (allelefrequencies.net), we used the $S_{167–180}$ HLA class II tetramer to evaluate 14 of the mRNA vaccine study subjects with available blood and lymph node samples to empirically determine which individuals were HLA-DPB1*$04:01^+$ and thus had the $S_{167–180}$-specific $CD4^+$ T cell response. Nine of the 14 subjects had a detectable $S_{167–180}$-specific response in peripheral blood following boost vaccination. Next, we tracked and characterized this response over time in frozen PBMC (N = 8 subjects) and frozen lymph node FNA samples (N = 6 unique lymph nodes from 5 subjects) from a convenience sample of the subjects who had sufficient sample remaining for analysis. The $S_{167–180}$-specific $CD4^+$ T cell response peaked in peripheral blood 28 days after primary vaccination, 7 days after vaccine boost, and remained present in the blood at detectable frequencies through the entire study interval (Figures 3A and 3B). Most $S_{167–180}$-specific $CD4^+$ T cells circulating in peripheral blood exhibited a $CD45RO^+CCR7^-$ effector memory surface phenotype similar to what we observed in SARS-CoV-2-convalescent donors (Figure 3C). A subset of tetramer-positive $CD4^+$ T cells in the first 35 days following primary vaccination exhibited an activated surface phenotype characterized by upregulation of both CD38 and HLA-DR (Figure 3D). This activated $CD4^+$ T cell phenotype disappeared by day 60 post-primary vaccination. Most circulating $S_{167–180}$-specific $CD4^+$ T cells expressed both PD1 and ICOS at high levels on days 21 and 28 following primary vaccination with a gradual decrease in the mean fluorescent intensity of PD1 and ICOS throughout the remaining study interval to a level more consistent with that found on the majority of circulating $CD4^+$ T cells in line with resolution of T cell activation (Figure 3E). A subset of $S_{167–180}$-specific $CD4^+$ T cells accounting for approximately 5%–15% of the total number of circulating $S_{167–180}$-specific $CD4^+$ T cells exhibited the $CXCR5^+PD1^+$ circulating T_{FH} phenotype (Figure 3F). These circulating $S_{167–180}$-specific T_{FH} cells peaked 28 days after primary vaccination, 7 days after vaccine boost, and then decreased over time, becoming difficult to detect in the blood of some subjects by the final study time point (Figure 3G). We evaluated the expression of the Th1-associated chemokine receptor CXCR3 on the surface of $S_{167–180}$-specific $CD4^+$ T cells from a single subject with available sample and noted that most of the $S_{167–180}$-specific cells expressed CXCR3 but not CXCR5 at days 21 and 28 following primary vaccination (Figure S6). Collectively, these results demonstrate that the circulating $S_{167–180}$-specific $CD4^+$ T cell population exhibits a dynamic surface phenotype over time with a general bias toward surface phenotypes that do not include circulating T_{FH}.

In contrast to circulating populations of T_{FH} cells, the frequency of $S_{167–180}$-specific $CD4^+$ T_{FH} cells remained high in the draining axillary lymph node through at least day 60 following primary vaccination and persisted at high frequency in three of the five study subjects through day 200 following primary vaccination—more than 170 days following vaccine boost (Figure 4). The prolonged persistence of S-specific T_{FH} cells that we report here in the draining axillary lymph nodes corresponds well with the long-lived GC B cell responses recently reported in the same cohort of subjects (Turner et al., 2021). The vast majority of $S_{167–180}$-specific $CD4^+$ T cells in lymph node FNA samples co-expressed CXCR5

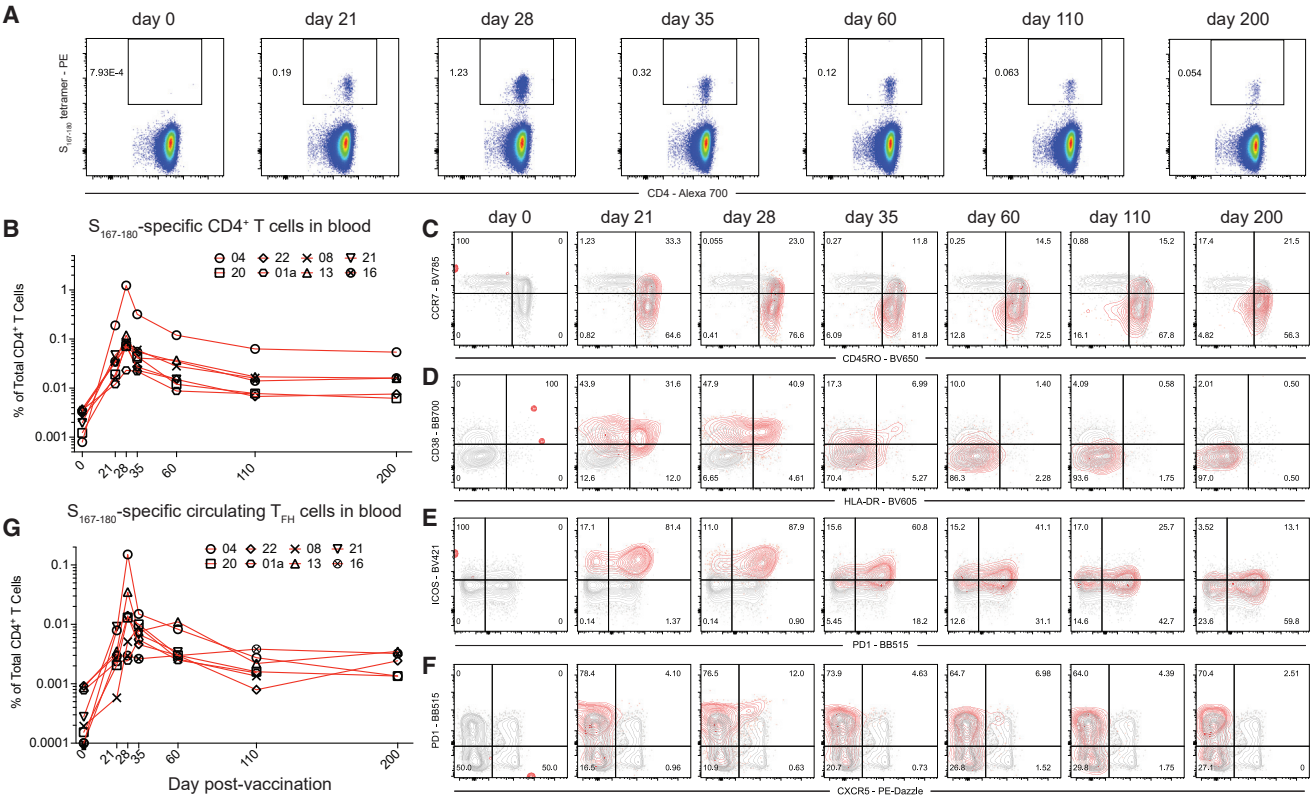

Figure 3. $S_{167–180}$ response in peripheral blood following BNT162b2 vaccination

(A) Representative flow cytometry plots of $S_{167–180}$ tetramer staining following vaccination of subject 04. Frequency displayed is the percent of live $CD3^+CD4^+$ T cells in the blood that are tetramer positive.

(B) The frequency of $S_{167–180}$ $tetramer^+$ cells in the blood over time in 8 of the study subjects with available PBMC from most time points.

(C–F) Surface phenotype of circulating $S_{167–180}$ $tetramer^+$ cells over time. Representative flow cytometry overlay plots from subject 04 showing total $CD4^+$ T cell (gray contours) and tetramer-positive (red contours) populations. (C) The majority of $S_{167–180}$ $tetramer^+$ cells retain an "effector memory" ($CD45RO^+CCR7^-$) surface phenotype following vaccination. (D) A subset of $S_{167–180}$ $tetramer^+$ cells undertake an "activated" surface phenotype ($HLA\text{-}DR^+CD38^+$) in the 2 weeks following vaccination. (E) ICOS and PD-1 are upregulated on the majority of $S_{167–180}$ $tetramer^+$ cells prior to and 7 days following boost vaccination. (F) A small subset of $S_{167–180}$ $tetramer^+$ cells undertake a "circulating T_{FH}" surface phenotype ($CXCR5^+PD1^+$) following boost vaccination, but the majority of circulating $S_{167–180}$ $tetramer^+$ cells do not exhibit this phenotype.

(G) $S_{167–180}$ $tetramer^+CXCR5^+PD1^+$ cells as a percentage of total live $CD3^+CD4^+$ T cells over time.

and PD1, surface markers of T_{FH} cells, throughout the study interval (Figure 4A). Furthermore, the frequency of $S_{167–180}$-specific $CD4^+$ T cells in the FNA samples remained consistently high or even increased as the frequency of $S_{167–180}$-specific $CD4^+$ T cells in the peripheral blood contracted. These lymph node T_{FH} responses remained at a high frequency until the conclusion of the GC response at day 200 in 2 of the 5 subjects (Figure 4B).

Next, we examined the frequency of $S_{167–180}$-specific $CD4^+$ T cells in the total $CXCR5^+PD1^+$ T_{FH} population in both the blood and the lymph nodes over time. We found that this population rapidly expanded in the blood—peaking at day 28 after primary vaccination, 7 days after vaccine boost—and then became challenging to detect by days 110 and 200 (Figure 4C) as we had previously noted when examining this population as a proportion of total $CD4^+$ T cells in Figure 3G. In contrast, the frequency of the $S_{167–180}$-specific T_{FH} population remained consistently elevated within the total T_{FH} population over time in the lymph node—until the resolution of the lymph node GC response at day 200 in 2 of the 5 subjects (Figure 4C; Table S1). Together, these results demonstrate that a small subset of antigen-specific $CD4^+$ T cells circulating in peripheral blood following vaccination develop a surface phenotype consistent with circulating T_{FH} cells. This coincides with the development of T_{FH} cells in the draining lymph node with the same antigen specificity. Furthermore, while this population nearly disappears from circulating blood 110 days after vaccination, the response remains constant in the lymph node in the presence of an ongoing GC reaction. Overall, our findings are consistent with the development of diverse lineages of effector $CD4^+$ T cells—those that express a surface phenotype consistent with T_{FH} and those that do not—from a single population of naive $CD4^+$ T cells that share a common TCRα chain motif. This is consistent with observations in mouse models where the specificity and duration of the TCR/peptide/MHC class II interaction correlated with the overall balance between Th1 and T_{FH} cell frequency (Tubo et al., 2013).

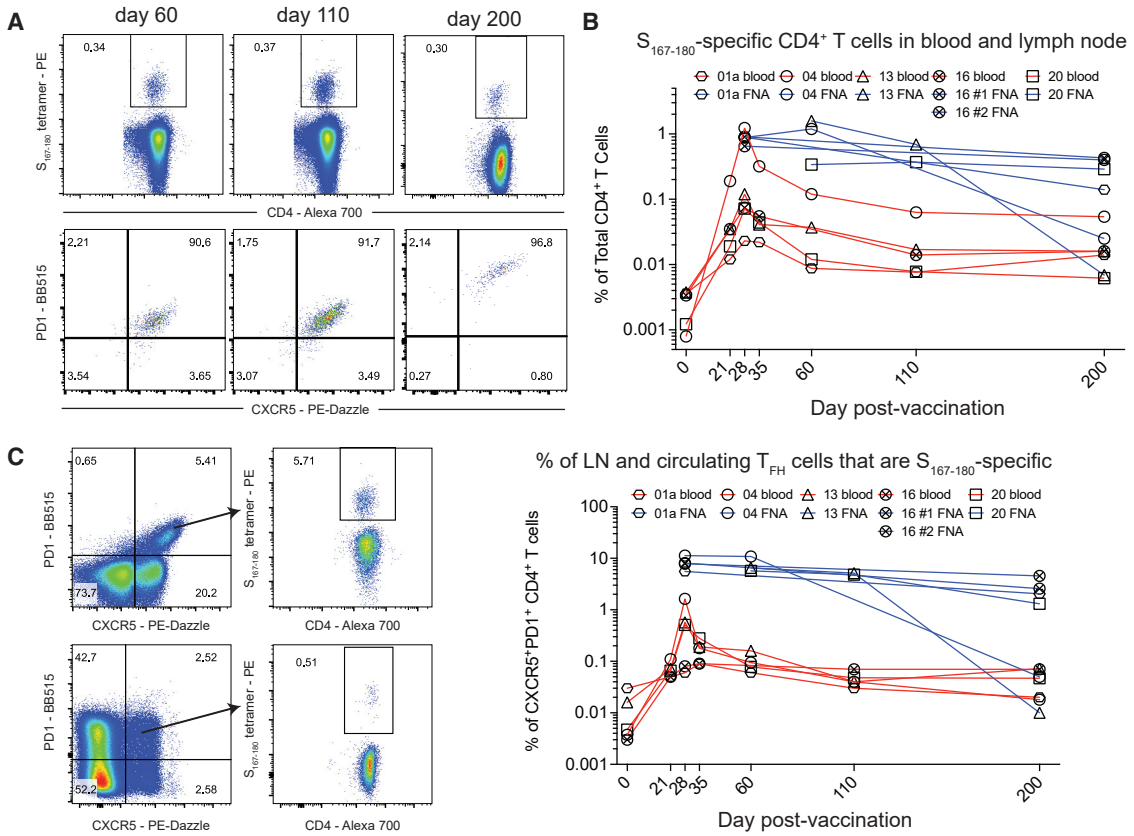

Figure 4. $S_{167–180}$ response in the draining lymph node following BNT162b2 vaccination

(A) Representative flow cytometry plots of subject 20 demonstrating the frequency of $S_{167–180}$ tetramer$^+$ cells expressed as a percentage of total CD4$^+$ T cells in the lymph node FNA sample (top row). The bottom row demonstrates CXCR5 and PD1 surface expression on the gated $S_{167–180}$ tetramer$^+$ cells from the row above.

(B) The percentage of total CD4$^+$ T cells that are $S_{167–180}$ tetramer$^+$ in blood (red lines) and FNA (blue lines) in matched samples taken at the same time points from subjects with available sample.

(C) The percentage of CXCR5$^+$PD1$^+$ T cells that are $S_{167–180}$ tetramer$^+$ over time in both the blood (red lines) and FNA (blue lines).

Diverse clonal populations of T_{FH} in the human GC persist at a consistent frequency over time

We subsequently quantified the contribution of the $S_{167–180}$ T_{FH} population to the broader clonotypic diversity of the T_{FH} population found in the lymph node from four of the subjects by further analyzing the TCR sequencing data from sorted T_{FH} cells generated for Figure 1C. The clonotypes that compose the $S_{167–180}$ response made up the largest percentage of total clonotypes present in the lymph node for three of the four subjects and composed the second highest percentage of clonotypes in the fourth subject (Figure 5A). This underscores the importance of the immunodominant HLA-DPB1*04-restricted $S_{167–180}$ response in the total SARS-CoV-2-specific T_{FH} cell response of HLA-DPB1*04$^+$ vaccinees, who make up approximately 40%–50% of the world's population.

To elucidate the clonal composition of the T_{FH} cell response over time, we sequenced samples from two time points that were available from these individuals. Three subjects were sequenced at day 60 and day 110 post-primary vaccination and one subject was sequenced at day 28 and day 60 following primary vaccination (Table S3). Three of the subjects exhibited evidence of ongoing antigen-specific T_{FH} responses associated with GC responses in our earlier flow cytometry experiments at all tested time points (Figure 4), while there were insufficient remaining samples from subject #22 for this analysis. In support of our observations in the flow cytometry analysis of the $S_{167–180}$ population, we found a positive correlation between the frequency of a large number of the TCRα clonotype sequences at the two time points (Figure 5B), including the known $S_{167–180}$-specific TCR clonotypes (Figure 5B, red data points). This was especially true of the clonotypes found at the highest frequency in each FNA sample, which are those that are most likely to represent antigen-specific clonotypes due to their increased presence in the lymph node following vaccination. This positive correlation means that many of these clonotypes were found at similar frequency at both tested time points. Therefore, the maintenance of consistently high-frequency antigen-specific T_{FH} cell responses over time during an ongoing antigen-specific GC B cell response (Turner et al., 2021) that we observed in the context of the $S_{167–180}$-specific CD4$^+$ T_{FH} response (Figure 4C) is generalizable to other clonally related and presumably antigen-specific T_{FH} populations in the human lymph node following

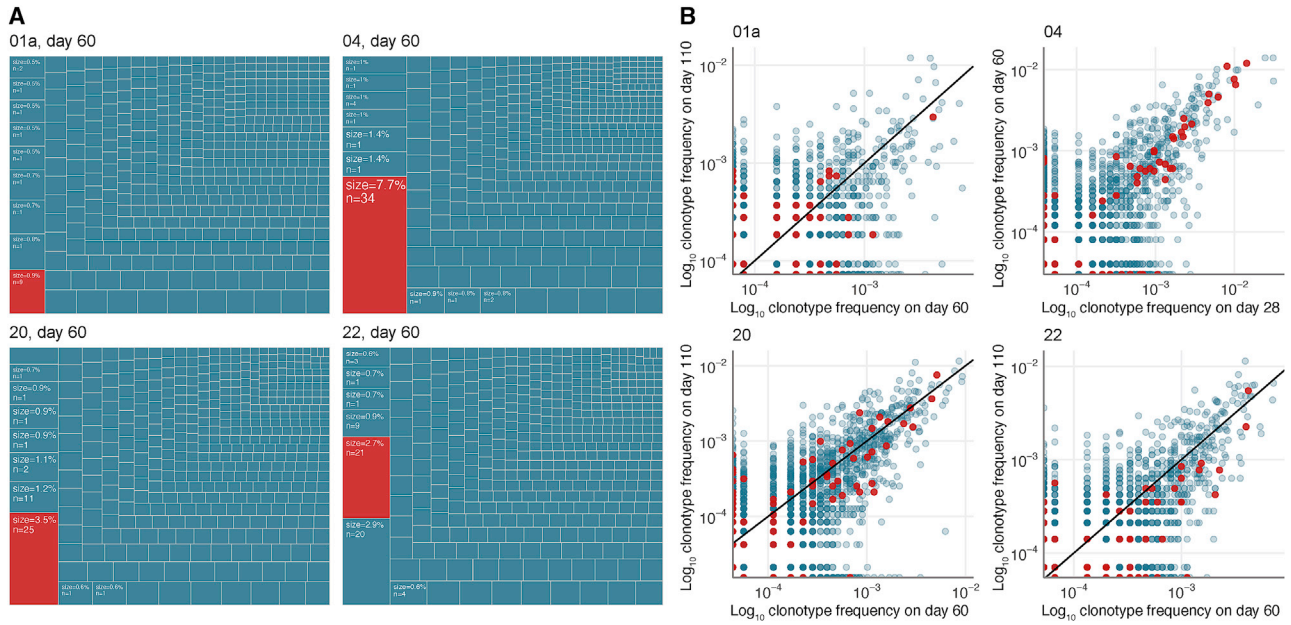

Figure 5. The $S_{167–180}$ response composes a large fraction of the T_{FH} repertoire and maintains a consistent frequency over time

(A) Abundance of the $S_{167–180}$-specific clones (red boxes) in the lymph node T_{FH} repertoires of 4 donors on day 60 after mRNA vaccination. Listed frequency is the frequency of the examined clonal group (defined as a cluster from Figure 1B) out of the total clonal sequences in the sorted T_{FH} sample. The $S_{167–180}$ response is the largest T_{FH} response in 3 of the 4 examined HLA-DPB1*04$^+$ subjects lymph nodes.

(B) Clonotype frequencies of sequenced sorted CXCR5$^+$PD1$^+$ T_{FH} repertoires from lymph nodes sampled at two separate time points. Each dot corresponds to an individual TCRα clonotype. Frequencies are shown in log scale. Red dots correspond to $S_{167–180}$-specific clones based on the known α-chain motif.

BNT162b2 vaccination. Our data support a model whereby the antigen-specific human GC T_{FH} cell response is maintained at a relatively consistent and high frequency in the setting of an active and ongoing GC reaction, rather than a response that peaks or dynamically changes in frequency over time.

DISCUSSION

In this report, we show that the BNT162b2 COVID-19 mRNA vaccine induces robust and persistent T_{FH} responses in the draining lymph nodes of vaccinated individuals. Indirect evidence has existed for some time that robust CD4$^+$ T cell responses are required for the generation of high-titer neutralizing antibody responses following COVID-19 infection or mRNA vaccination. This includes data showing a lack of seroconversion in individuals with uncontrolled HIV and extremely low CD4$^+$ T cell counts during vaccination (Touizer et al., 2021) as well as several reports that have demonstrated a lack of seroconversion to the standard two-dose BNT162b2 regimen in individuals subjected to T-cell-focused immunosuppressive regimens following solid organ transplantation (Kamar et al., 2021). Our current results provide strong and direct evidence that a high-magnitude, antigen-specific CD4$^+$ T cell response in the draining lymph nodes is present during the development of high-titer neutralizing antibody responses in the setting of COVID-19 mRNA vaccination.

The temporal relationship we observe between the early appearance and then disappearance of $S_{167–180}$-specific CD4$^+$ T cells exhibiting a circulating T_{FH} phenotype in the blood at the same time that we observe T_{FH} cells in the draining lymph node suggests a complex relationship between these two populations of cells. Our present data support a model of human T_{FH} cell development whereby phenotypically heterogeneous, or even plastic, antigen-specific CD4$^+$ T cell populations induced by primary vaccination are activated and expand in the lymph node and circulating compartments prior to the development and migration of more specialized subpopulations that co-express CXCR5 and PD1 to the lymph node GC (Crotty, 2018). In our $S_{167–180}$ tetramer data, most $S_{167–180}$-specific CD4$^+$ T cells in the blood did not exhibit a circulating T_{FH} phenotype even at the day 28 post-primary vaccination peak of circulating $S_{167–180}$-specific T_{FH}. Very few $S_{167–180}$-specific memory CD4$^+$ T cells maintained in blood more than 3 months after vaccination expressed both CXCR5 and PD1. Nevertheless, $S_{167–180}$-specific T_{FH} cells compose the largest or second largest S-specific T_{FH} population in the lymph node of all evaluated subjects despite the near absence of these cells in the circulating blood at the same late time points. Together, our data support a model whereby clonal populations of circulating CD4$^+$ T cells develop into many different lineages, including the T_{FH} cell lineage. Furthermore, we were unable to find a strong, direct relationship between the cells known as circulating T_{FH} (circulating antigen-specific CD4$^+$CXCR5$^+$PD1$^+$ cells) and the presence of large populations of clonally matched antigen-specific T_{FH} cells participating in an ongoing GC in the lymph node. This is in contrast to data from a study of matched tonsil and blood samples in subjects who were not recently vaccinated or infected where they found substantial clonal overlap between tonsil T_{FH} populations and circulating T_{FH} populations but little overlap between tonsil T_{FH} populations and circulating non-

T_{FH} populations (Brenna et al., 2020). Further studies are required to determine the relationship between populations of circulating and lymph-node-resident T_{FH} cells in both the steady state and following vaccination, as these systems are quite distinct.

The discovered DPB1*04-restricted $S_{167–180}$ response is notable for the extraordinarily constrained TCRα sequence diversity. This single TCRα motif is immediately obvious with even cursory inspection of bulk $CD4^+$ TCR sequences from vaccinated or infected individuals. Surprisingly, no prominent TCRβ motif is observed in any of our sequencing of this response, emphasizing the importance of the α-chain in certain instances of specific epitope recognition (Dash et al., 2017; Minervina et al., 2020; Shomuradova et al., 2020). The high prevalence of DPB1*04 in worldwide populations means that this response is likely immunodominant across multiple populations and contributes significantly to the measured responses in many studies, though its restriction has not been previously assigned. Thus far, none of the prevalent variant SARS-CoV-2 strains including the delta and omicron variants have acquired stable mutations in this peptide sequence.

In conclusion, we find that mRNA vaccine technology has an exceptional ability to induce high-frequency antigen-specific B cell (Turner et al., 2021) and antigen-specific $CD4^+$ T_{FH} cell responses in the human lymph node following prime-boost administration. These characteristics underlie the development of high-titer neutralizing antibodies and protection from infection in vaccinated individuals. The selective enhancement of lymph node T_{FH} responses induced by vaccine regimens represents a broad strategy for improving future vaccines.

Limitations of the study

Our study has several limitations, including the small number of included subjects, the relatively young age of the included participants, and the lack of comprehensive epitope mapping beyond the immunodominant response that we identified. Furthermore, the complex nature of both the vaccination rollout during the ongoing pandemic and the FNA sampling procedure itself eliminated our ability to sample lymph nodes prior to vaccination and at earlier time points following the primary vaccination. Furthermore, although we repeatedly sampled some axillary lymph nodes until the apparent conclusion of the GC response in those nodes, we were unable to sample non-draining control lymph nodes at distal sites. Limitations in the small number of available cells from the FNA procedure precluded total S-specific T cell response measurement in the LN samples using assays such as AIM or ICS. In addition, limitations to the convalescent patient sample study precluded longitudinal analysis of these responses in the previously infected patient cohort. There are several questions that we did not address that will be useful topics for future studies, including the extent of clonal overlap between the blood and lymph node $CD4^+$ T cell compartments, and the transcriptional profiles of the lymph node T_{FH} response over the long period of clonal stability.

CONSORTIA

The members of the SJTRC Study Team are Jeremie H. Estepp, Stacey Schultz-Cherry, Maureen A. McGargill, Aditya Gaur, James Hoffman, Motomi Mori, Li Tang, Elaine Tuomanen, Richard Webby, Randall T. Hayden, Hana Hakim, Diego R. Hijano, Kim J. Allison, E. Kaitlynn Allen, Resha Bajracharya, Walid Awad, Lee-Ann Van de Velde, Brandi L. Clark, Taylor L. Wilson, Aisha Souquette, Ashley Castellaw, Ronald H. Dallas, Ashleigh Gowen, Thomas P. Fabrizio, Chun-Yang Lin, David C. Brice, Sean Cherry, Ericka Kirkpatrick Roubidoux, Valerie Cortez, Pamela Freiden, Nicholas Wohlgemuth, and Kendall Whitt.

STAR★METHODS

Detailed methods are provided in the online version of this paper and include the following:

- KEY RESOURCES TABLE
- RESOURCE AVAILABILITY
  - Lead contact
  - Materials availability
  - Data and code availability
- EXPERIMENTAL MODEL AND SUBJECT DETAILS
  - Human subjects
- METHOD DETAILS
  - Cell sorting and flow cytometry
  - Jurkat cell line generation
  - Jurkat peptide stimulation
  - Peptide stimulation and intracellular cytokine staining of SJTRC samples
  - Activation-induced marker (AIM) assay
  - Monomer generation
  - Tetramer generation and staining of Jurkat cells
  - Tetramer staining of SJTRC samples and scTCR sequencing
  - Bulk repertoire generation
  - Public TCR repertoire datasets
- QUANTIFICATION AND STATISTICAL ANALYSIS
  - TCR repertoire analysis
  - Statistical analysis

SUPPLEMENTAL INFORMATION

Supplemental information can be found online at https://doi.org/10.1016/j.cell.2021.12.026.

ACKNOWLEDGMENTS

The authors would like to thank the study participants for their invaluable contribution to this work. We also thank Greig Lennon from St. Jude Immunology flow core for his help with FACS, Hartwell Center at St. Jude Children's Research Hospital for high-throughput sequencing, and Carmen Llerna for assistance in HLA-DP4 protein purification. This study was funded in part by the Washington University Institute for Clinical and Translational Sciences grant UL1TR002345 from the National Center for Advancing Translational Sciences (NCATS) of the National Institutes of Health (NIH) (P.A.M.). J.R. is supported by an Australian Research Council Laureate Fellowship. K.K. was supported by the NHMRC Leadership Investigator Fellowship (#1173871), and T.H.O.N. was supported by the NHMRC Emerging Leadership Level 1 Investigator Fellowship (#1194036). This work was funded by ALSAC at St. Jude; the Center for Influenza Vaccine Research for High-Risk Populations (CIVR-HRP) contract number 75N93019C00052 (P.G.T. and K.K.); the St. Jude Center of Excellence for Influenza Research and Surveillance (P.G.T.) contract number HHSN272201400006C; and the St. Jude Center of Excellence for Influenza Research and Response (P.G.T.) contract numbers 75N93021C00016,

U01AI150747, U01AI144616-02S1, and R01AI136514 (P.G.T.). The Ellebedy laboratory was supported by NIAID grants U01AI141990 and U01AI150747, NIAID Centers of Excellence for Influenza Research and Surveillance contracts HHSN272201400006C and HHSN272201400008C, and by NIAID Collaborative Influenza Vaccine Innovation Centers contract 75N93019C00051. The contents of this publication are solely the responsibility of the authors and do not necessarily represent the official views of the NIAID or NIH.

AUTHOR CONTRIBUTIONS

Conceptualization: P.A.M., A.A.M., M.V.P., P.G.T., and A.H.E.; methodology: P.A.M., A.A.M., M.V.P., J.S.T., J.P., J.C.C., M.K.K., S.A.T., J.A.O., R.M.P., P.G.T., and A.H.E.; investigation: P.A.M., A.A.M., M.V.P., J.S.T., W.K., E.K., J.P., A.J. Schmitz, T.L., A.H., A.M.K., R.C.M., J.C.C., T.H.O.N., L.C.R., E.R., K.A.R., A.J. Sant, T.S., W.D.M., and S.A.T.; formal analysis: P.A.M., A.A.M., M.V.P., and J.C.C.; visualization: P.A.M., A.A.M., M.V.P., and R.C.M.; resources: SJTRC Study Team; Data curation: J.C.C., J.W., and SJTRC Study Team; funding acquisition: P.A.M., P.G.T., and A.H.E.; supervision: P.A.M., S.A.T., J.A.O., R.M.P., K.K., J.R., P.G.T., and A.H.E.; writing – original draft: P.A.M., A.A.M., and M.V.P.; writing – review & editing: all co-authors.

DECLARATION OF INTERESTS

The Ellebedy laboratory received funding under sponsored research agreements that are unrelated to the data presented in the current study from Emergent BioSolutions and from AbbVie. A.H.E. has received consulting payments from Mubadala Investment Company, InBios International, and Fimbrion Therapeutics and is the founder of ImmuneBio Consulting. P.G.T. has consulted and/or received honoraria and travel support from Illumina, Johnson and Johnson, and 10X Genomics. P.G.T. serves on the Scientific Advisory Board of Immunoscape and Cytoagents. The authors have applied for patents covering some aspects of these studies.

INCLUSION AND DIVERSITY

We worked to ensure gender balance in the recruitment of human subjects. We worked to ensure ethnic or other types of diversity in the recruitment of human subjects.

Received: September 6, 2021
Revised: November 12, 2021
Accepted: December 17, 2021
Published: December 23, 2021

REFERENCES

Al Kaabi, N., Zhang, Y., Xia, S., Yang, Y., Al Qahtani, M.M., Abdulrazzaq, N., Al Nusair, M., Hassany, M., Jawad, J.S., Abdalla, J., et al. (2021). Effect of 2 inactivated SARS-CoV-2 vaccines on symptomatic COVID-19 infection in adults: A randomized clinical trial. JAMA *326*, 35–45.

Anderson, E.J., Rouphael, N.G., Widge, A.T., Jackson, L.A., Roberts, P.C., Makhene, M., Chappell, J.D., Denison, M.R., Stevens, L.J., Pruijssers, A.J., et al. (2020). Safety and immunogenicity of SARS-CoV-2 mRNA-1273 vaccine in older adults. N. Engl. J. Med. *383*, 2427–2438.

Bacher, P., Rosati, E., Esser, D., Martini, G.R., Saggau, C., Schiminsky, E., Dargvainiene, J., Schröder, I., Wieters, I., Khodamoradi, Y., et al. (2020). Low-avidity CD4+ T cell responses to SARS-CoV-2 in unexposed individuals and humans with severe COVID-19. Immunity *53*, 1258–1271, e5.

Baden, L.R., El Sahly, H.M., Essink, B., Kotloff, K., Frey, S., Novak, R., Diemert, D., Spector, S.A., Rouphael, N., Creech, C.B., et al. (2021). Efficacy and safety of the mRNA-1273 SARS-CoV-2 vaccine. N. Engl. J. Med. *384*, 403–416.

Bolotin, D.A., Poslavsky, S., Mitrophanov, I., Shugay, M., Mamedov, I.Z., Putintseva, E.V., and Chudakov, D.M. (2015). MiXCR: software for comprehensive adaptive immunity profiling. Nat. Methods *12*, 380–381.

Brenna, E., Davydov, A.N., Ladell, K., McLaren, J.E., Bonaiuti, P., Metsger, M., Ramsden, J.D., Gilbert, S.C., Lambe, T., Price, D.A., et al. (2020). CD4+ T follicular helper cells in human tonsils and blood are clonally convergent but divergent from non-Tfh CD4+ cells. Cell Rep *30*, 137–152, e5.

Chen, R.E., Zhang, X., Case, J.B., Winkler, E.S., Liu, Y., VanBlargan, L.A., Liu, J., Errico, J.M., Xie, X., Suryadevara, N., et al. (2021). Resistance of SARS-CoV-2 variants to neutralization by monoclonal and serum-derived polyclonal antibodies. Nat. Med. *27*, 717–726.

Corbett, K.S., Nason, M.C., Flach, B., Gagne, M., O' Connell, S., Johnston, T.S., Shah, S.N., Edara, V.V., Floyd, K., Lai, L., et al. (2021). Immune correlates of protection by mRNA-1273 immunization against SARS-CoV-2 infection in nonhuman primates (immunology). bioRxiv. https://doi.org/10.1101/2021.04.20.440647.

Crotty, S. (2011). Follicular helper CD4 T cells (T FH). Annu. Rev. Immunol. *29*, 621–663.

Crotty, S. (2018). Do memory CD4 T cells keep their cell-type programming: plasticity versus fate commitment? Complexities of interpretation due to the heterogeneity of memory CD4 T cells, including T follicular helper cells. Cold Spring Harb. Perspect. Biol. *10*, a032102.

Dash, P., Fiore-Gartland, A.J., Hertz, T., Wang, G.C., Sharma, S., Souquette, A., Crawford, J.C., Clemens, E.B., Nguyen, T.H.O., Kedzierska, K., et al. (2017). Quantifiable predictive features define epitope-specific T cell receptor repertoires. Nature *547*, 89–93.

Dykema, A.G., Zhang, B., Woldemeskel, B.A., Garliss, C.C., Cheung, L.S., Choudhury, D., Zhang, J., Aparicio, L., Bom, S., Rashid, R., et al. (2021). Functional characterization of CD4+ T cell receptors crossreactive for SARS-CoV-2 and endemic coronaviruses. J. Clin. Invest. *131*, e146922.

Egorov, E.S., Merzlyak, E.M., Shelenkov, A.A., Britanova, O.V., Sharonov, G.V., Staroverov, D.B., Bolotin, D.A., Davydov, A.N., Barsova, E., Lebedev, Y.B., et al. (2015). Quantitative profiling of immune repertoires for minor lymphocyte counts using unique molecular identifiers. J. Immunol. *194*, 6155–6163.

Glanville, J., Huang, H., Nau, A., Hatton, O., Wagar, L.E., Rubelt, F., Ji, X., Han, A., Krams, S.M., Pettus, C., et al. (2017). Identifying specificity groups in the T cell receptor repertoire. Nature *547*, 94–98.

Good-Jacobson, K.L., Chen, Y., Voss, A.K., Smyth, G.K., Thomas, T., and Tarlinton, D. (2014). Regulation of germinal center responses and B-cell memory by the chromatin modifier MOZ. Proc. Natl. Acad. Sci. USA *111*, 9585–9590.

Jackson, L.A., Anderson, E.J., Rouphael, N.G., Roberts, P.C., Makhene, M., Coler, R.N., McCullough, M.P., Chappell, J.D., Denison, M.R., Stevens, L.J., et al. (2020). An mRNA vaccine against SARS-CoV-2 – preliminary report. N. Engl. J. Med. *383*, 1920–1931.

Jensen, K.K., Andreatta, M., Marcatili, P., Buus, S., Greenbaum, J.A., Yan, Z., Sette, A., Peters, B., and Nielsen, M. (2018). Improved methods for predicting peptide binding affinity to MHC class II molecules. Immunology *154*, 394–406.

Kamar, N., Abravanel, F., Marion, O., Couat, C., Izopet, J., and Del Bello, A. (2021). Three doses of an mRNA Covid-19 vaccine in solid-organ transplant recipients. N Engl J Med *385*, 661–662. https://doi.org/10.1056/NEJMc2108861.

Khoury, D.S., Cromer, D., Reynaldi, A., Schlub, T.E., Wheatley, A.K., Juno, J.A., Subbarao, K., Kent, S.J., Triccas, J.A., and Davenport, M.P. (2021). Neutralizing antibody levels are highly predictive of immune protection from symptomatic SARS-CoV-2 infection. Nat. Med. *27*, 1205–1211.

Kim, W., Zhou, J.Q., Sturtz, A.J., Horvath, S.C., Schmitz, A.J., Lei, T., Kalaidina, E., Thapa, M., Alsoussi, W.B., Haile, A., et al. (2021). Germinal centre-driven maturation of B cell response to SARS-CoV-2 vaccination. bioRxiv. https://doi.org/10.1101/2021.10.31.466651.

Logunov, D.Y., Dolzhikova, I.V., Shcheblyakov, D.V., Tukhvatulin, A.I., Zubkova, O.V., Dzharullaeva, A.S., Kovyrshina, A.V., Lubenets, N.L., Grousova, D.M., Erokhova, A.S., et al. (2021). Safety and efficacy of an rAd26 and rAd5 vector-based heterologous prime-boost COVID-19 vaccine: an interim analysis of a randomised controlled phase 3 trial in Russia. Lancet *397*, 671–681.

Loyal, L., Braun, J., Henze, L., Kruse, B., Dingeldey, M., Reimer, U., Kern, F., Schwarz, T., Mangold, M., Unger, C., et al. (2021). Cross-reactive CD4+ T cells enhance SARS-CoV-2 immune responses upon infection and vaccination. Science *374*, eabh1823.

Meckiff, B.J., Ramírez-Suástegui, C., Fajardo, V., Chee, S.J., Kusnadi, A., Simon, H., Eschweiler, S., Grifoni, A., Pelosi, E., Weiskopf, D., et al. (2020). Imbalance of regulatory and cytotoxic SARS-CoV-2-reactive CD4+ T cells in COVID-19. Cell *183*, 1340–1353, e16.

Minervina, A.A., Pogorelyy, M.V., Komech, E.A., Karnaukhov, V.K., Bacher, P., Rosati, E., Franke, A., Chudakov, D.M., Mamedov, I.Z., Lebedev, Y.B., et al. (2020). Primary and secondary anti-viral response captured by the dynamics and phenotype of individual T cell clones. eLife *9*, e53704.

Minervina, A.A., Komech, E.A., Titov, A., Bensouda Koraichi, M., Rosati, E., Mamedov, I.Z., Franke, A., Efimov, G.A., Chudakov, D.M., Mora, T., et al. (2021a). Longitudinal high-throughput TCR repertoire profiling reveals the dynamics of T-cell memory formation after mild COVID-19 infection. eLife *10*, e63502.

Minervina, A.A., Pogorelyy, M.V., Kirk, A.M., Allen, E.K., Allison, K.J., Lin, C.-Y., Brice, D.C., Zhu, X., Vegesana, K., Wu, G., et al. (2021b). Convergent epitope-specific T cell responses after SARS-CoV-2 infection and vaccination. medRxiv. https://doi.org/10.1101/2021.07.12.21260227.

Niehrs, A., Garcia-Beltran, W.F., Norman, P.J., Watson, G.M., Hölzemer, A., Chapel, A., Richert, L., Pommerening-Röser, A., Körner, C., Ozawa, M., et al. (2019). A subset of HLA-DP molecules serve as ligands for the natural cytotoxicity receptor NKp44. Nat. Immunol. *20*, 1129–1137.

Nolan, S., Vignali, M., Klinger, M., Dines, J.N., Kaplan, I.M., Svejnoha, E., Craft, T., Boland, K., Pesesky, M., Gittelman, R.M., et al. (2020). A large-scale database of T-cell receptor beta (TCRβ) sequences and binding associations from natural and synthetic exposure to SARS-CoV-2. Res. Sq. https://doi.org/10.21203/rs.3.rs-51964/v1.

Painter, M.M., Mathew, D., Goel, R.R., Apostolidis, S.A., Pattekar, A., Kuthuru, O., Baxter, A.E., Herati, R.S., Oldridge, D.A., Gouma, S., et al. (2021). Rapid induction of antigen-specific CD4+ T cells is associated with coordinated humoral and cellular immunity to SARS-CoV-2 mRNA vaccination. Immunity *54*, 2133–2142, e3.

Peng, Y., Mentzer, A.J., Liu, G., Yao, X., Yin, Z., Dong, D., Dejnirattisai, W., Rostron, T., Supasa, P., Liu, C., et al. (2020). Broad and strong memory CD4+ and CD8+ T cells induced by SARS-CoV-2 in UK convalescent individuals following COVID-19. Nat. Immunol. *21*, 1336–1345.

Pogorelyy, M.V., Minervina, A.A., Shugay, M., Chudakov, D.M., Lebedev, Y.B., Mora, T., and Walczak, A.M. (2019). Detecting T cell receptors involved in immune responses from single repertoire snapshots. PLoS Biol *17*, e3000314.

Polack, F.P., Thomas, S.J., Kitchin, N., Absalon, J., Gurtman, A., Lockhart, S., Perez, J.L., Pérez Marc, G., Moreira, E.D., Zerbini, C., et al. (2020). Safety and efficacy of the BNT162b2 mRNA Covid-19 vaccine. N. Engl. J. Med. *383*, 2603–2615.

Qi, H. (2016). T follicular helper cells in space-time. Nat. Rev. Immunol. *16*, 612–625.

Ripperger, T.J., and Bhattacharya, D. (2021). Transcriptional and metabolic control of memory B cells and plasma cells. Annu. Rev. Immunol. *39*, 345–368.

Sacha, J.B., and Watkins, D.I. (2010). Synchronous infection of SIV and HIV in vitro for virology, immunology and vaccine-related studies. Nat. Protoc. *5*, 239–246.

Sadoff, J., Gray, G., Vandebosch, A., Cárdenas, V., Shukarev, G., Grinsztejn, B., Goepfert, P.A., Truyers, C., Fennema, H., Spiessens, B., et al. (2021). Safety and efficacy of single-dose Ad26.COV2.S vaccine against Covid-19. N. Engl. J. Med. *384*, 2187–2201.

Scally, S.W., Petersen, J., Law, S.C., Dudek, N.L., Nel, H.J., Loh, K.L., Wijeyewickrema, L.C., Eckle, S.B.G., van Heemst, J., Pike, R.N., et al. (2013). A molecular basis for the association of the HLA-DRB1 locus, citrullination, and rheumatoid arthritis. J. Exp. Med. *210*, 2569–2582.

Shomuradova, A.S., Vagida, M.S., Sheetikov, S.A., Zornikova, K.V., Kiryukhin, D., Titov, A., Peshkova, I.O., Khmelevskaya, A., Dianov, D.V., Malasheva, M., et al. (2020). SARS-CoV-2 epitopes are recognized by a public and diverse repertoire of human T cell receptors. Immunity *53*, 1245–1257, e5.

Shugay, M., Britanova, O.V., Merzlyak, E.M., Turchaninova, M.A., Mamedov, I.Z., Tuganbaev, T.R., Bolotin, D.A., Staroverov, D.B., Putintseva, E.V., Plevova, K., et al. (2014). Towards error-free profiling of immune repertoires. Nat. Methods *11*, 653–655.

Stadlbauer, D., Amanat, F., Chromikova, V., Jiang, K., Strohmeier, S., Arunkumar, G.A., Tan, J., Bhavsar, D., Capuano, C., Kirkpatrick, E., et al. (2020). SARS-CoV-2 seroconversion in humans: a detailed protocol for a serological assay, antigen production, and test setup. Curr. Protoc. Microbiol. *57*, e100.

Tarke, A., Sidney, J., Kidd, C.K., Dan, J.M., Ramirez, S.I., Yu, E.D., Mateus, J., da Silva Antunes, R., Moore, E., Rubiro, P., et al. (2021). Comprehensive analysis of T cell immunodominance and immunoprevalence of SARS-CoV-2 epitopes in COVID-19 cases. Cell Rep. Med. *2*, 100204.

Touizer, E., Alrubayyi, A., Rees-Spear, C., Fisher-Pearson, N., Griffith, S.A., Muir, L., Pellegrino, P., Waters, L., Burns, F., Kinloch, S., et al. (2021). Failure to seroconvert after two doses of BNT162b2 SARS-CoV-2 vaccine in a patient with uncontrolled HIV. Lancet HIV *8*, e317–e318.

Tubo, N.J., Pagán, A.J., Taylor, J.J., Nelson, R.W., Linehan, J.L., Ertelt, J.M., Huseby, E.S., Way, S.S., and Jenkins, M.K. (2013). Single naive CD4+ T cells from a diverse repertoire produce different effector cell types during infection. Cell *153*, 785–796.

Turner, J.S., O'Halloran, J.A., Kalaidina, E., Kim, W., Schmitz, A.J., Zhou, J.Q., Lei, T., Thapa, M., Chen, R.E., Case, J.B., et al. (2021). SARS-CoV-2 mRNA vaccines induce persistent human germinal centre responses. Nature *596*, 109–113.

Turner, J.S., Zhou, J.Q., Han, J., Schmitz, A.J., Rizk, A.A., Alsoussi, W.B., Lei, T., Amor, M., McIntire, K.M., Meade, P., et al. (2020). Human germinal centres engage memory and naive B cells after influenza vaccination. Nature *586*, 127–132.

Ueno, H., Banchereau, J., and Vinuesa, C.G. (2015). Pathophysiology of T follicular helper cells in humans and mice. Nat. Immunol. *16*, 142–152.

Verbeke, R., Lentacker, I., De Smedt, S.C., and Dewitte, H. (2021). The dawn of mRNA vaccines: the COVID-19 case. J. Control. Release *333*, 511–520.

Victora, G.D., and Nussenzweig, M.C. (2012). Germinal centers. Annu. Rev. Immunol. *30*, 429–457.

Voysey, M., Clemens, S.A.C., Madhi, S.A., Weckx, L.Y., Folegatti, P.M., Aley, P.K., Angus, B., Baillie, V.L., Barnabas, S.L., Bhorat, Q.E., et al. (2021). Safety and efficacy of the ChAdOx1 nCoV-19 vaccine (AZD1222) against SARS-CoV-2: an interim analysis of four randomised controlled trials in Brazil, South Africa, and the UK. Lancet *397*, 99–111.

Walsh, E.E., Frenck, R.W., Falsey, A.R., Kitchin, N., Absalon, J., Gurtman, A., Lockhart, S., Neuzil, K., Mulligan, M.J., Bailey, R., et al. (2020). Safety and immunogenicity of two RNA-based Covid-19 vaccine candidates. N. Engl. J. Med. *383*, 2439–2450.

Wang, G.C., Dash, P., McCullers, J.A., Doherty, P.C., and Thomas, P.G. (2012). T cell receptor αβ diversity inversely correlates with pathogen-specific antibody levels in human cytomegalovirus infection. Sci. Transl. Med. *4*, 128ra42.

Wang, P., Nair, M.S., Liu, L., Iketani, S., Luo, Y., Guo, Y., Wang, M., Yu, J., Zhang, B., Kwong, P.D., et al. (2021a). Antibody resistance of SARS-CoV-2 variants B.1.351 and B.1.1.7. Nature *593*, 130–135.

Wang, Z., Schmidt, F., Weisblum, Y., Muecksch, F., Barnes, C.O., Finkin, S., Schaefer-Babajew, D., Cipolla, M., Gaebler, C., Lieberman, J.A., et al. (2021b). mRNA vaccine-elicited antibodies to SARS-CoV-2 and circulating variants. Nature *592*, 616–622.

Weisel, F.J., Zuccarino-Catania, G.V., Chikina, M., and Shlomchik, M.J. (2016). A temporal switch in the germinal center determines differential output of memory B and plasma cells. Immunity *44*, 116–130.

Widge, A.T., Rouphael, N.G., Jackson, L.A., Anderson, E.J., Roberts, P.C., Makhene, M., Chappell, J.D., Denison, M.R., Stevens, L.J., Pruijssers, A.J., et al. (2021). Durability of responses after SARS-CoV-2 mRNA-1273 vaccination. N. Engl. J. Med. *384*, 80–82.

Wu, K., Werner, A.P., Koch, M., Choi, A., Narayanan, E., Stewart-Jones, G.B.E., Colpitts, T., Bennett, H., Boyoglu-Barnum, S., Shi, W., et al. (2021). Serum neutralizing activity elicited by mRNA-1273 vaccine. N. Engl. J. Med. *384*, 1468–1470.

STAR★METHODS

KEY RESOURCES TABLE

REAGENT or RESOURCE	SOURCE	IDENTIFIER
Antibodies		
CD4 Alexa Fluor 700 (clone SK3)	BioLegend	cat#: 344622; RRID: AB_2563150
CD19 PE (clone HIB19)	BioLegend	cat#: 302208; RRID: AB_314238
CXCR5 PE-Dazzle 594 (clone J252D4)	BioLegend	cat#: 356928; RRID: AB_2563689
PD1 BB515 (clone EH12.1)	BD Biosciences	cat#: 564494; RRID: AB_2738827
IgG BV480 (goat polyclonal)	Jackson ImmunoResearch	cat#: 109-685-098; RRID: AB_2721846
IgA FITC (clone M24A)	Millipore	cat#: CBL114F; RRID: AB_92852
CD45 A532 (clone HI30)	Thermo	cat#: 58-0459-42; RRID: AB_11218673
CD38 BB700 (clone HIT2)	BD Biosciences	cat#: 566445; RRID: AB_2744375
CD20 Pacific Blue (clone 2H7)	BioLegend	cat#: 980204; RRID: AB_2632618
CD27 BV510 (clone O323)	BioLegend	cat#: 302836; RRID: AB_2562086
CD8 BV570 (clone RPA-T8)	BioLegend	cat#: 301038; RRID: AB_2563213
IgM BV605 (clone MHM-88)	BioLegend	cat#: 314524; RRID: AB_2562374
HLA-DR BV650 (clone L243)	BioLegend	cat#: 307650; RRID: AB_2563828
CD19 BV750 (clone HIB19)	BioLegend	cat#: 302262; RRID: AB_2810434
IgD PE-Cy5 (clone IA6-2)	BioLegend	cat#: 348250; RRID: AB_2876661
CD14 PerCP (clone HCD14)	BioLegend	cat#: 325632; RRID: AB_2563328
CD71 PE-Cy7 (clone CY1G4)	BioLegend	cat#: 334112; RRID: AB_2563119
CD4 Spark 685 (clone SK3)	BioLegend	cat#: 344658; RRID: AB_2819981
CD3 APC-Fire 810 (clone SK7)	BioLegend	cat#: 344858; RRID: AB_2860895
FoxP3 BV421 (clone 206D)	BioLegend	cat#: 320124; RRID: AB_2565972
Ki-67 BV711 (clone Ki-67)	BioLegend	cat#: 350516; RRID: AB_2563861
Tbet BV785 (clone 4B10)	BioLegend	cat#: 644835; RRID: AB_2721566
Bcl6 PE (clone K112-91)	BD Biosciences	cat#: 561522; RRID: AB_10717126
BLIMP1 Alexa Fluor 700 (clone 646702)	R&D Systems	cat#: IC36081N
CD4 Alexa Fluor 700 (clone SK3)	BioLegend	cat#: 344622; RRID: AB_2563150
CD45RO BV650 (clone UCHL1)	BioLegend	cat#: 304232; RRID: AB_2563462
CCR7 BV785 (clone G043H7)	BioLegend	cat#: 353230; RRID: AB_2563630
HLA-DR BV605 (clone L243)	BioLegend	cat#: 307640; RRID: AB_2561913
ICOS BV421 (clone C398.4A)	BioLegend	cat#: 313524; RRID: AB_2562545
IgD PE-Cy7 (clone IA6-2)	BioLegend	cat#: 348210; RRID: AB_10680462
CD3 Alexa Fluor 700 (clone HIT3a)	BioLegend	cat#: 300324; RRID: AB_493739
CD4 PerCP (clone SK3)	BioLegend	cat#: 344624; RRID: AB_2563326
CD45RO APC-Fire 750 (clone UCHL1)	BioLegend	cat#: 304250; RRID: AB_2616717
CXCR3 BV650 (clone G025H7)	BioLegend	cat#: 353730; RRID: AB_2563870
TCR-beta chain APC-Fire 750 (clone H57-597)	BioLegend	cat#: 109246; RRID: AB_2629697
CD3 BV421 (clone SK7)	BioLegend	cat#: 344834; RRID: AB_2565675
anti-human CD28 purified (clone CD28.2)	BD Biosciences	cat#: 555725; RRID: AB_396068
anti-human CD49d purified (clone 9F10)	BD Biosciences	cat#: 555501; RRID: AB_2130052
human Fc block (clone Fc1.3216)	BD Biosciences	cat#: 564220; RRID: AB_2869554
Human TruStain FcX	BioLegend	cat#: 422302; RRID: AB_2818986
CD19 BV510 (clone HIB19)	BioLegend	cat#: 302242; RRID: AB_2561668
CD69 PerCP-eFluor 710 (clone FN50)	eBioscience	cat#: 460699-42; RRID: AB_2573694
CXCR5 Super Bright 436 (clone MU5UBEE)	eBioscience	cat#: 62-9185-42; RRID: AB_2724064

(*Continued on next page*)

Continued

REAGENT or RESOURCE	SOURCE	IDENTIFIER
CD45RA eFluor 450 (clone HI100)	eBioscience	cat#: 48-0458-42; RRID: AB_1272059
CD8 BV570 (clone RPA-T8)	BioLegend	cat#: 301038; RRID: AB_2563213
CD3 BV750 (clone SK7)	BioLegend	cat#: 344846; RRID: AB_2800923
CD4 BB515 (clone SK3)	BD Biosciences	cat#: 565996; RRID: AB_2739447
PD-1 FITC (clone EH12.2H7)	BioLegend	cat#: 329904; RRID: AB_940479
ICOS PerCP-Cy5.5 (clone C398.4A)	BioLegend	cat#: 313518; RRID: AB_10641280
CD69 PE-Cy7 (clone FN50)	BioLegend	cat#: 310912; RRID: AB_314847
TCR gamma/delta Alexa Fluor 647 (clone B1)	BioLegend	cat#: 331214; RRID: AB_1089210
anti-human IFN-gamma BV480 (clone B27)	BD Biosciences	cat#: 566100; RRID: AB_2739503
anti-human TNF-alpha BV605 (clone Mab11)	BioLegend	cat#: 502936; RRID: AB_2563884
anti-human IL-17A BV785 (clone BL168)	BioLegend	cat#: 512338; RRID: AB_2566765
anti-human IL-21 PE (clone 3A3-N2)	BioLegend	cat#: 513004; RRID: AB_2249025
anti-human IL-2 APC (clone MQ1-17H12)	eBioscience	cat#: 17-7029-82; RRID: AB_469492
CD40 (clone HB14)	Miltenyi Biotec	cat#: 130-094-133; RRID: AB_10839704
Co-stimulatory antibodies (CD28/CD49d, clones L293/L25))	BD Biosciences	cat#: 347690; RRID: AB_647457
CD40L BV605 (clone 24-31)	BioLegend	cat#: 310826; RRID: AB_2563832
CD3 FITC (clone SK7)	BioLegend	cat#: 344804; RRID: AB_2043993
CD200 PerCP-Cy5.5 (clone OX-104)	BioLegend	cat#: 329216; RRID: AB_2563251
CD8 APC (clone SK1)	BioLegend	cat#: 344722; RRID: AB_2075388
CD45RA BV421 (clone HI100)	BioLegend	cat#: 304130; RRID: AB_10965547
CD4 BV711 (clone OKT4)	BioLegend	cat#: 317440; RRID: AB_2562912
CD3 PerCP-Cy5.5 (clone OKT3)	BioLegend	cat#: 317336; RRID: AB_2561628
CCR7 FITC (clone G043H7)	BioLegend	cat#: 353216; RRID: AB_10916386
Biological samples		
Peripheral blood human samples after SARS-CoV-2 infection	St. Jude Tracking of Viral and Host Factors Associated with COVID-19 study (SJTRC, NCT04362995)	N/A
Peripheral blood human samples after BNT162b2 vaccination	St. Jude Tracking of Viral and Host Factors Associated with COVID-19 study (SJTRC, NCT04362995)	N/A
Peripheral blood and matched lymph node samples after BNT162b2 vaccination	WU-368 study (approval #2020-12-081)	N/A
Chemicals, peptides, and recombinant proteins		
Recombinant SARS-CoV-2 Spike protein – Biotin conjugated	Stadlbauer et al., 2020	N/A
Recombinant SARS-CoV-2 Spike protein – Alexa Fluor 647 conjugated	Stadlbauer et al., 2020	N/A
Recombinant SARS-CoV-2 Spike protein – Alexa Fluor 488 conjugated	Stadlbauer et al., 2020	N/A
PE-labeled HLA-DPB1*04:01 $S_{167-180}$ tetramer	This paper	N/A
Brilliant Staining buffer	BD Biosciences	N/A
streptavidin APC-Fire 750	BioLegend	cat#: 566349
True-Nuclear Transcription Factor Buffer Set	BioLegend	cat#: 405250
Zombie Aqua	BioLegend	cat#: 423106
Zombie NIR Fixable Viability Kit	BioLegend	cat#: 424401
Lenti-X Concentrator	Clontech	cat#: 631232

(*Continued on next page*)

Continued

REAGENT or RESOURCE	SOURCE	IDENTIFIER
1x Cell Stimulation cocktail	eBioscience	cat#: 00-4970-93
Ghost Dye Violet 510 Viability Dye	Tonbo Biosciences	cat#: 13-0870-T100
CTFEYVSQPFLMDLE peptide (>95% purity)	This paper	N/A
TFEYVSQPFLMDLE peptide	This paper	N/A
SARS-CoV-2 Prot_S Complete Peptivator	Miltenyi	cat#: 130-127-951
NQKLIANQF peptide (>95% purity)	Minervina et al., 2020	N/A
GolgiPlug	BD Biosciences	cat#: 555029
Fixation/Permeabilization Solution kit	BD Biosciences	cat#: 554715
streptavidin PE	BioLegend	cat#: 405204
Critical commercial assays		
AllType NGS 11-Loci Amplification Kit	One Lambda	cat#: ALL-11LX
SuperScript VILO cDNA Synthesis kit	Invitrogen	cat#: 11754250
SmartScribe Reverse Transcriptase	Takara	cat#: 639538
Q5 Hot Start High-Fidelity DNA Polymerase	NEB	cat#: M0493
Deposited data		
Processed TCR repertoire sequencing data	This paper	GEO: GSE183393
Raw TCR repertoire sequencing data	This paper	SRA: SRP335569
Experimental models: Cell lines		
293T	ATCC	cat#: CRL-3216
Jurkat 76.7 (variant of TCR-null Jurkat 76.7 cells that expresses human CD8 and an NFAT-GFP reporter)	gift from Wouter Scheper	N/A
Oligonucleotides		
5' – template switch adapter (SmartNNNa): AAGCAGUGGTAUCAACGCAGAGUNNNNUNNNNUNNNNUCTT(rG)4	Egorov et al., 2015	N/A
Primer for cDNA synthesis, human TCR alpha chain mRNA, C-region (ACR_st4): GTCTAGCACAGTTTTGTC	Egorov et al., 2015	N/A
Primer for cDNA synthesis, human TCR beta chain mRNA, C-region (BCR4short): GTATCTGGAGTCATTGA	Egorov et al., 2015	N/A
Forward primer for PCR step1, anneals on the switch adapter(M1ss): AAGCAGTGGTATCAACGCA	Egorov et al., 2015	N/A
Nested reverse primer for PCR step1, TCR alpha, C-region (ACR_st1):GTCACTGGATTTAGAGTC	Egorov et al., 2015	N/A
Nested reverse primer for PCR step1, TCR beta, C-region (BC2uniR):TGCTTCTGATGGCTCAAACAC	Egorov et al., 2015	N/A
Barcoded forward PCR step 2 primer (M1s_i): (N)4(XXXXX)CAGTGGTATCAACGCAGAG	Egorov et al., 2015	N/A
Barcoded reverse PCR step 2 primer (TCR alpha): (N)4(XXXXX)GGGTCAGGGTTCTGGATAT	Egorov et al., 2015	N/A
Barcoded reverse PCR step 2 primer (TCR beta): (N)4(XXXXX)ACACSTTKTTCAGGTCCTC	Egorov et al., 2015	N/A
huTRBV2ext: TCGATGATCAATTCTCAGTTG	Wang et al., 2012	N/A
huTRBV3ext: CAAAATACCTGGTCACACAG	Wang et al., 2012	N/A
huTRBV4ext: TCGCTTCTCACCTGAATG	Wang et al., 2012	N/A
huTRBV5-1_4ext: GATTCTCAGGKCKCCAGTTC	Wang et al., 2012	N/A
huTRBV5-5_8ext: GTACCAACAGGYCCTGGGT	Wang et al., 2012	N/A

(*Continued on next page*)

Continued

REAGENT or RESOURCE	SOURCE	IDENTIFIER
huTRBV6-1_3,5_9ext: ACTCAGACCCCAAAATTCC	Wang et al., 2012	N/A
huTRBV6-4ext: ACTGGCAAAGGAGAAGTCC	Wang et al., 2012	N/A
huTRBV7-1_3ext: TRTGATCCAATTTCAGGTCA	Wang et al., 2012	N/A
huTRBV7-4_9extnew: CGSWTCTYTGCAGARAGGC	Wang et al., 2012	N/A
huTRBV9ext: GATCACAGCAACTGGACAG	Wang et al., 2012	N/A
huTRBV10-1ext: CAGAGCCCAAGACACAAG	Wang et al., 2012	N/A
huTRBV10-2ext: ACCTTGATGTGTCACCAGAC	Wang et al., 2012	N/A
huTRBV10-3ext: CAGAGCCCAAGACACAAG	Wang et al., 2012	N/A
huTRBV11ext: CGATTTTCTGCAGAGACGC	Wang et al., 2012	N/A
huTRBV12ext: ARGTGACAGARATGGGACAA	Wang et al., 2012	N/A
huTRBV13ext: AGCGATAAAGGAAGCATCC	Wang et al., 2012	N/A
huTRBV14ext: CCAACAATCGATTCTTAGCTG	Wang et al., 2012	N/A
huTRBV15extnew: AGTGACCCTGAGTTGTTCTC	Wang et al., 2012	N/A
huTRBV16ext1: GTCTTTGATGAAACAGGTATGC	Wang et al., 2012	N/A
huTRBV17ext_new: CAGACCCCCAGACACAAG	Wang et al., 2012	N/A
huTRBV18ext: CATAGATGAGTCAGGAATGCC	Wang et al., 2012	N/A
huTRBV19ext: AGTTGTGAACAGAATTTGAACC	Wang et al., 2012	N/A
huTRBV20ext: AAGTTTCTCATCAACCATGC	Wang et al., 2012	N/A
huTRBV23ext: GCGATTCTCATCTCAATGC	Wang et al., 2012	N/A
huTRBV24ext: CCTACGGTTGATCTATTACTCC	Wang et al., 2012	N/A
huTRBV25ext: ACTACACCTCATCCACTATTCC	Wang et al., 2012	N/A
huTRBV27,28ext: TGGTATCGACAAGACCCAG	Wang et al., 2012	N/A
huTRBV29ext: TTCTGGTACCGTCAGCAAC	Wang et al., 2012	N/A
huTRBV30ext: TCCAGCTGCTCTTCTACTCC	Wang et al., 2012	N/A
huTRBCext: TAGAACTGGACTTGACAGCG	Wang et al., 2012	N/A
huTRAV1ext: AACTGCACGTACCAGACATC	Wang et al., 2012	N/A
huTRAV2ext_new: GATGTGCACCAAGACTCC	Wang et al., 2012	N/A
huTRAV3ext: AAGATCAGGTCAACGTTGC	Wang et al., 2012	N/A
huTRAV4ext: CTCCATGGACTCATATGAAGG	Wang et al., 2012	N/A
huTRAV5ext: CTTTTCCTGAGTGTCCGAG	Wang et al., 2012	N/A
huTRAV6ext: CACCCTGACCTGCAACTATAC	Wang et al., 2012	N/A
huTRAV7ext_new: GCAAAATACAGGGATGGG	Wang et al., 2012	N/A
huTRAV8-1ext: CTCACTGGAGTTGGGATG	Wang et al., 2012	N/A
huTRAV8-3ext: CACTGTCTCTGAAGGAGCC	Wang et al., 2012	N/A
huTRAV8-2,4ext: GCCACCCTGGTTAAAGG	Wang et al., 2012	N/A
huTRAV8-6ext: GAGCTGAGGTGCAACTACTC	Wang et al., 2012	N/A
huTRAV8-7ext_new2: CTAACAGAGGCCACCCAG	Wang et al., 2012	N/A
huTRAV9-1_2ext: TGGTATGTCCAATATCCTGG	Wang et al., 2012	N/A
huTRAV10ext: CAAGTGGAGCAGAGTCCTC	Wang et al., 2012	N/A
huTRAV12-1_3ext: CARTGTTCCAGAGGGAGC	Wang et al., 2012	N/A
huTRAV13-1ext: CATCCTTCAACCCTGAGTG	Wang et al., 2012	N/A
huTRAV13-2ext_new: CAGCGCCTCAGACTACTTC	Wang et al., 2012	N/A
huTRAV14ext: AAGATAACTCAAACCCAACCAG	Wang et al., 2012	N/A
huTRAV16ext: AGTGGAGCTGAAGTGCAAC	Wang et al., 2012	N/A
huTRAV17ext: GGAGAAGAGGATCCTCAGG	Wang et al., 2012	N/A
huTRAV18ext_new3: TCCAGTATCTAAACAAAGAGCC	Wang et al., 2012	N/A
huTRAV19ext: AGGTAACTCAAGCGCAGAC	Wang et al., 2012	N/A
huTRAV20ext: CACAGTCAGCGGTTTAAGAG	Wang et al., 2012	N/A

(*Continued on next page*)

Continued

REAGENT or RESOURCE	SOURCE	IDENTIFIER
huTRAV21ext: TTCCTGCAGCTCTGAGTG	Wang et al., 2012	N/A
huTRAV22ext: GTCCTCCAGACCTGATTCTC	Wang et al., 2012	N/A
huTRAV23ext_new: TGCTTATGAGAACACTGCG	Wang et al., 2012	N/A
huTRAV24ext: CTCAGTCACTGCATGTTCAG	Wang et al., 2012	N/A
huTRAV25ext_new: GGACTTCACCACGTACTGC	Wang et al., 2012	N/A
huTRAV26-1ext: GCAAACCTGCCTTGTAATC	Wang et al., 2012	N/A
huTRAV26-2ext: AGCCAAATTCAATGGAGAG	Wang et al., 2012	N/A
huTRAV27ext: TCAGTTTCTAAGCATCCAAGAG	Wang et al., 2012	N/A
huTRAV29ext: GCAAGTTAAGCAAAATTCACC	Wang et al., 2012	N/A
huTRAV30ext: CAACAACCAGTGCAGAGTC	Wang et al., 2012	N/A
huTRAV34ext: AGAACTGGAGCAGAGTCCTC	Wang et al., 2012	N/A
huTRAV35ext: GGTCAACAGCTGAATCAGAG	Wang et al., 2012	N/A
huTRAV36ext: GAAGACAAGGTGGTACAAAGC	Wang et al., 2012	N/A
huTRAV38ext: GCACATATGACACCAGTGAG	Wang et al., 2012	N/A
huTRAV39ext: CTGTTCCTGAGCATGCAG	Wang et al., 2012	N/A
huTRAV40ext_new: GCATCTGTGACTATGAACTGC	Wang et al., 2012	N/A
huTRAV41ext: AATGAAGTGGAGCAGAGTCC	Wang et al., 2012	N/A
huTRACext: GACCAGCTTGACATCACAG	Wang et al., 2012	N/A
Recombinant DNA		
pLVX-EF1α-IRES-Puro	Clontech	cat#: 631253
TCR_4.1-mCherry	This paper	N/A
TCR_6.3-mCherry	This paper	N/A
psPAX2 packaging plasmid	gift from Didier Trono	Addgene plasmid #12260; RRID: Addgene_12260
pMD2.G envelope plasmid	gift from Didier Trono	Addgene plasmid #12259; RRID: Addgene_12259
Software and algorithms		
FlowJo v10.7.1	BD Biosciences	https://www.flowjo.com/solutions/flowjo/downloads
SpectroFlo v2.2	Cytek	https://cytekbio.com/pages/spectro-flo
R v. 4.0.1		https://www.r-project.org
Prism v9.1.0	GraphPad Software	https://graphpad.com
Biorender		https://biorender.com
MiGEC v. 1.2.7	Bolotin et al., 2015	https://github.com/mikessh/migec
MiXCR v. 3.0.3	Shugay et al., 2014	https://github.com/milaboratory/mixcr
data.table R package v. 1.14.0		https://github.com/Rdatatable/data.table/wiki
stringdist R package v. 0.9.6.3		https://github.com/markvanderloo/stringdist
igraph R package v. 1.2.6		https://igraph.org/r/
gephi v. 0.9.2		https://gephi.org
ggplot2 R package v. 3.3.3		https://cran.r-project.org/web/packages/ggplot2/index.html

RESOURCE AVAILABILITY

Lead contact

Further information and requests for resources and reagents should be directed to and will be fulfilled by the lead contact, Ali H. Ellebedy (ellebedy@wustl.edu).

Materials availability

The HLA-DPB1*04 $S_{167-180}$ HLA class II tetramer has been submitted to the NIH tetramer core facility (tetramer.yerkes.emory.edu). No other new unique reagents were generated in this study.

Data and code availability

- Processed TCR sequencing data have been submitted to the GEO database:GSE183393, and the raw sequencing data have been submitted to the SRA database: SRP335569. All sequencing data are publicly available as of the date of publication. Any raw flow cytometry data not available in the supplemental tables will be shared by the lead contact upon request.
- This paper does not report original code.
- Any additional information required to reanalyze the data reported in this paper is available from the lead contact upon request.

EXPERIMENTAL MODEL AND SUBJECT DETAILS

Human subjects

Human subjects who elected to receive the BNT162b2 mRNA vaccine were recruited into this prospective observational study. Written informed consent was obtained from each subject. The study was approved by the Washington University in St. Louis Institutional Review Board (approval # 2020-12-081). Details of the entire study cohort have been previously reported (Turner et al., 2021). The age and sex of the subjects included in the present study are listed in Table 1. Draining axillary lymph nodes ipsilateral to the deltoid vaccination site were located with ultrasound and sampled with multiple passes of 6 separate 25-gauge needles under real-time ultrasound guidance (Turner et al., 2020). Each needle was flushed with 3 mL of R10 (RPMI, 1640 supplemented with 10% FBS and 100 U/mL penicillin-streptomycin) and the 3 separate 1 mL rinses of R10. Red blood cells were lysed with 1xACK (Sacha and Watkins, 2010) and then washed with P2 (1xPBS supplemented with 2% FBS and 2 mM EDTA). FNA samples were immediately stained for flow cytometry or cryopreserved in freezing media (10% dimethylsulfoxide and 90% FBS). Two subjects – 07 and 15 – received their BNT162b2 vaccine in the contralateral arm to the initial axillary lymph node FNA site. Subject 15 then had FNA performed on two lymph nodes, one ipsilateral and the other contralateral to the deltoid vaccination for all FNA samples completed starting on day 28. Matched blood samples from the same time-points were obtained by standard phlebotomy into EDTA anti-coagulated tubes and PBMC were prepared by density gradient centrifugation over Ficoll 1077 (GE). PBMC were treated with 1xACK for 5 minutes to lyse residual red blood cells before washing with R10 and immediate use in flow cytometry experiments or cryopreservation in freezing media.

For $S_{167-180}$ tetramer validation and ICS experiments we used PBMC from SARS-CoV-2 convalescent and vaccinated donors obtained as a part of the St. Jude Tracking of Viral and Host Factors Associated with COVID-19 study (SJTRC, NCT04362995); a prospective, IRB-approved, longitudinal cohort study of St. Jude Children's Research Hospital adult ($\geq$18 years old) employees. Participants were screened for SARS-CoV-2 infection by PCR approximately weekly when on St. Jude campus. For this study, we utilized the convalescent blood draw for SARS-CoV-2 infected individuals (3-8 weeks post diagnosis) as well as post-vaccination blood draws for SARS-CoV-2 naive individuals. Blood samples were collected in 8 mL CPT tubes; and PBMC were isolated and frozen within 24 hours of collection. HLA typing of each included SJTRC participant was performed using the AllType NGS 11-Loci Amplification Kit (One Lambda; Lot 013) according to manufacturer's instructions. Resulting libraries were sequenced on MiSeq lane at 150x150bp. HLA types were called using the TypeStream Visual Software from One Lambda.

METHOD DETAILS

Cell sorting and flow cytometry

Fresh or frozen PBMC and/or FNA samples were washed and re-suspended in P2. For sorting of T_{FH} populations from frozen FNA samples in Figures 1B and 5, cells were stained with CD4 Alexa Fluor 700 (SK3, BioLegend), CD19 PE (HIB19, BioLegend), CXCR5 PE-Dazzle 594 (J252D4, BioLegend), PD1 BB515 (EH12.1, BD Horizon), and Zombie Aqua (BioLegend) for a total of 30 minutes on ice. Cells were then washed twice with P2 and live, singlet, $CD4^+CD19^-CXCR5^+PD1^+$ cells were sorted on a FACSAria II into Trizol before being immediately frozen on dry ice.

To analyze antigen-specific B cell populations, we generated labeled recombinant soluble SARS-CoV-2 spike protein as previously described (Stadlbauer et al., 2020). A mammalian cell codon-optimized nucleotide sequence coding for the soluble ectodomain of the spike protein of SARS-CoV-2 (GenBank: MN908947.3, amino acids 1-1213) including a C-terminal thrombin cleavage site, T4 foldon trimerization domain, and hexahistidine tag was cloned into mammalian expression vector pCAGGS. The spike protein sequence was modified to remove the polybasic cleavage site (RRAR to A), and two pre-fusion stabilizing proline mutations were introduced (K986P and V987P, wild type numbering). Recombinant S was produced in Expi293F cells (ThermoFisher) by transfection with purified DNA using the ExpiFectamine 293 Transfection Kit (ThermoFisher). Supernatants from transfected cells were harvested 3 days post-transfection, and recombinant proteins were purified using Ni-NTA agarose (ThermoFisher), then buffer exchanged into phosphate buffered saline (PBS) and concentrated using Amicon Ultracel centrifugal filters (EMD Millipore). For flow cytometry staining, recombinant S was labeled with DyLight 488-NHS ester, Alexa Fluor 647-NHS ester or biotinylated using the EZ-Link Micro

NHS-PEG4-Biotinylation Kit (Thermo Fisher); excess DyLight 488 was removed using 40-kDa Zeba desalting columns; excess Alexa Fluor 647 and biotin were removed using 7-kDa Zeba desalting columns (Pierce).

In the bulk lymph node T_{FH} versus germinal center B cell experiment, FNA samples were stained in P2 for 30 minutes on ice with biotinylated and Alexa Fluor 647 conjugated recombinant soluble Spike proteins as well as PD-1 BB515 (EH12.1, BD Horizon). Cells were then washed twice with P2 and stained with IgG BV480 (goat polyclonal, Jackson ImmunoResearch), IgA FITC (M24A, Millipore), CD45 A532 (HI30, Thermo), CD38 BB700 (HIT2, BD Horizon), CD20 Pacific Blue (2H7, BioLegend, CD27 BV510 (O323, BioLegend), CD8 BV570 (RPA-T8, BioLegend), IgM BV605 (MHM-88, BioLegend), HLA-DR BV650 (L243, BioLegend), CD19 BV750 (HIB19, BioLegend), CXCR5 PE-Dazzle 594 (J252D4, BioLegend), IgD PE-Cy5 (IA6-2, BioLegend), CD14 PerCP (HCD14, BioLegend), CD71 PE-Cy7 (CY1G4, BioLegend), CD4 Spark685 (SK3, BioLegend), streptavidin APC-Fire750 (BioLegend), CD3 APC-Fire810 (SK7, BioLegend) and Zombie NIR (BioLegend) diluted in Brilliant Staining buffer (BD Horizon). Cells were then washed twice more with P2, fixed with the True Nuclear fixation kit (BioLegend) for 1 hour at room temperature, washed twice with True Nuclear Permeabilization/Wash buffer and then stained for 1 hour at room temperature with FoxP3 BV421 (206D, BioLegend), Ki-67 BV711 (Ki-67, BioLegend), Tbet BV785 (4B10, BioLegend), Bcl6 PE (K112-91, BD Pharmingen) and BLIMP1 Alexa Fluor 700 (646702, R&D Systems). Cells were then washed twice with True Nuclear Permeabilization/Wash buffer before acquisition on a Cytek Aurora spectral flow cytometer using SpectroFlo v2.2 software (Cytek) and analyzed using FlowJo software (BD).

In tetramer staining experiments cells were stained in P2 for 10 minutes on ice with PE-labeled HLA-DPB1*04:01 $S_{167\text{-}180}$ tetramer. Then, without washing away the tetramer, a master mix was added to the cells that included pre-titrated volumes of the following reagents: CD8 BV570 (RPA-T8, BioLegend) CD3 APC-Fire 810 (SK7, BioLegend) CD4 Alexa Fluor 700 (SK3, BioLegend) CD45RO BV650 (UCHL1, BioLegend) CCR7 BV785 (G043H7, BioLegend) CXCR5 PE-Dazzle 594 (J252D4, BioLegend) PD1 BB515 (EH12.1, BD Horizon) HLA-DR BV605 (L243, BioLegend) CD38 BB700 (HIT2, BD Horizon) ICOS BV421 (C398.4A, BioLegend) CD27 BV510 (O323, BioLegend) CD19 BV750 (HIB19, BioLegend) CD20 Pacific Blue (2H7, BioLegend) IgD PE-Cy7 (IA6-2, BioLegend) Zombie NIR (BioLegend) Spike protein conjugated to Alexa 647 and Spike protein conjugated to Alexa 488 and Brilliant Staining buffer (BD Horizon). Samples were then incubated on ice for an additional 30 minutes before they were washed twice with P2 and fixed in a final concentration of 1% paraformaldehyde for 15 minutes at room temperature. Samples were then run on a Cytek Aurora spectral flow cytometer using SpectroFlo v2.2 software (Cytek) and analyzed using FlowJo software (v10.8.0, BD). The alternative staining method used to incorporate CXCR3 evaluation in Figure S6 substituted the following antibodies into the panel listed above: CD3 Alexa Fluor 700 (HIT3a, BioLegend), CD4 PerCP (SK3, BioLegend), CD45RO APC-Fire 750 (UCHL1, BioLegend), and added CXCR3 BV650 (G025H7, BioLegend). Tetramer responses over time in Figures 3 and 4 were graphed in Prism (v9.1.0, GraphPad Software, LLC).

Jurkat cell line generation

For Jurkat cell line generation we selected a TCRα (TRAV35, CAGMNYGGSQGNLIF, TRAJ42) and two different TCRβ chains (TRBV4-1, CASSQGVGYTF, TRBJ1-2; TRBV6-3, CASSYRGAYGYTF, TRBJ1-2) from Bacher et al. Both TCRα and TCRβ chains were modified to use murine constant regions to facilitate surface expression (murine TRAC*01 and murine TRBC2*01). Two gBlock gene fragments were synthesized by Genscript to encode the modified TCRα chain, one of the modified TCRβ chains, and mCherry fluorescent protein, linked together by 2A sites. These sequences were cloned into the pLVX-EF1α-IRES-Puro lentiviral expression vector (Clontech). To generate the lentivirus we transfected 293T packaging cell line (ATCC CRL-3216) with the pLVX lentiviral vector containing TCR_4.1-mCherry or TCR_6.3-mCherry insert, psPAX2 packaging plasmid (Addgene plasmid #12260), and pMD2.G envelope plasmid (Addgene plasmid #12259). Viral supernatant was collected and concentrated using Lenti-X Concentrator 24- and 48-hours after the transfection (Clontech). Jurkat 76.7 cells (a gift from Wouter Scheper; variant of TCR-null Jurkat 76.7 cells that expresses human CD8 and an NFAT-GFP reporter) were transduced, then antibiotic selected for 1 week using 1 μg/mL puromycin in RPMI (Gibco) containing 10% FBS and 1% penicillin/streptomycin. Transduction of Jurkat cell line was confirmed by expression of mCherry, and surface TCR expression was confirmed via flow cytometry on a BD Fortessa using FACSDiva software using antibodies against mouse TCRβ constant region (APC-Fire750-conjugated, Biolegend, clone H57-597) and human CD3 (Brilliant Violet 421-conjugated, Biolegend, clone SK7). Flow data were analyzed in FlowJo software.

Jurkat peptide stimulation

Jurkat 76.7 cells expressing TCRs 4.1 and 6.3 ($2.5x10^5$) were co-cultured with PBMCs from SARS-CoV-2 naive DPB1*:04:01-positive donor ($6x10^5$) pulsed with 1 μM of peptide, 1 μg/mL each of anti-human CD28 and CD49d (BD Biosciences). An unstimulated (CD28, CD49d) and positive control (CD28, CD49d, 1X Cell Stimulation Cocktail, PMA/ionomycin; eBioscience) were included in each assay. Cells were incubated for 18 hours (37 $^{\circ}$C, 5% CO_2). After the incubation cells were washed twice with FACS buffer (PBS, 2% FBS, 1 mM EDTA), resuspended in 50 μL of FACS buffer, and then blocked using 1 μL human Fc-block (BD Biosciences). Cells were then stained with 1 μL Ghost Dye Violet 510 Viability Dye (Tonbo Biosciences) and a cocktail of fluorescent antibodies: 1 μL each of anti-human CD3 (Brilliant Violet 421-conjugated, Biolegend, clone SK7), anti-human CD69 (PerCP-eFluor710-conjugated, eBioscience, clone FN50), and anti-mouse TCRβ chain (APC/Fire750-conjugated, Biolegend, clone H57-597). Cells were incubated for 20 minutes at room temperature and then washed with a FACS buffer. Cells were analyzed by flow cytometry on a custom-configured BD Fortessa using FACSDiva software (Becton Dickinson). Flow cytometry data were analyzed using FlowJo software (BD Biosciences). Responsiveness to peptide stimulation was determined by measuring frequency of NFAT-GFP, CD69 and $\alpha\beta$TCR expression.

Peptide stimulation and intracellular cytokine staining of SJTRC samples

Donor PBMCs were thawed, suspended in RPMI 1640 supplemented with 10% heat-inactivated human AB serum (Gemini Bio-Products), 1% non-essential amino acids (Gibco), 1 mM sodium pyruvate (Gibco), and 100 U/mL penicillin-streptomycin (hR10), and plated at 2.5-4.0x10^5 cells/well in a 96-well U-bottom plate. PBMCs were stimulated with 5 μg/mL CTFEYVSQPFLMDLE peptide or left unstimulated and incubated at 37°C and 5% CO_2. After 12 h, 1x PMA/ionomycin (eBioscience) was added to positive control wells and GolgiPlug (BD Biosciences) was added at 1:1000 to all wells. Cells were incubated for an additional 6 h (for 18 h total), washed twice with FACS (PBS, 2% FBS, 1 mM EDTA), resuspended in 50 μL FACS containing 5 μL human Fc-block (Biolegend), and blocked for 15 min at RT. Cells were surface stained in an additional 50 uL FACS buffer containing 1 μL Ghost Dye Violet 510 Viability Dye (Tonbo Biosciences) and a cocktail of fluorescent anti-human antibodies: CXCR5 SuperBright 436 (Thermo, clone MU5UBEE), CD45RA eFluor 450 (Thermo, clone HI100), CD19 BV510 (Biolegend, clone HIB19), CD8 BV570 (Biolegend, clone RPA-T8), CD3 BV750 (Biolegend, clone SK7), CD4 BB515 (BD, clone SK3), PD1 FITC (Biolegend, clone EH12.2H7), ICOS PerCP/Cy5.5 (Biolegend, clone C398.4A), CD69 PE/Cy7 (Biolegend, clone FN50), and γδ TCR AlexaFluor 647 (Biolegend, clone B1) for 30 min at 4°C. Cells were washed twice with FACS buffer, fixed in Fix/Perm Solution (BD Biosciences) for 20 min at 4°C, and washed twice in Wash/Perm buffer (BD Biosciences). For detection of intracellular cytokines, cells were resuspended in 50 μL Perm/Wash buffer containing a cocktail of anti-human antibodies including IFNγ BV480 (BD Biosciences, clone B27), TNFα BV605 (Biolegend, clone MAb11), IL17 BV785 (Biolegend, clone BL168), IL21 PE (Biolegend, clone 3A3-N2), and IL2 APC (Thermo, clone MQ1-17H12) and were incubated for 30 min at 4°C. Cells were washed twice in FACS buffer and analyzed by flow cytometry on a Cytek Aurora spectral flow cytometer using SpectroFlo software (Cytek) and analyzed using FlowJo software (BD Biosciences). Responsiveness to peptide stimulation was determined by comparing the number of activated $CD4^+(CD69^+)$ T cells positive for IL2, IFNγ, or TNFα production per 10^6 PBMCs to matched unstimulated controls and presented as either fold change of stimulated over unstimulated, or number of stimulated cells after background subtraction of paired unstimulated controls.

Activation-induced marker (AIM) assay

Donor PBMCs were thawed, suspended in RPMI 1640 supplemented with 10% heat-inactivated human AB serum (Gemini Bio-Products), 1% non-essential amino acids (Gibco), 1 mM sodium pyruvate (Gibco), and 100 U/mL penicillin-streptomycin (hR10) and plated in replicate wells at 5.0x10^5 cells/well in a 96-well U-bottom plate. Cells were allowed to rest overnight in a 37°C and 5% CO_2 incubator. After 16 h, cells were treated with an anti-CD40 blocking antibody (Miltenyi, clone HB14) at a final concentration of 0.5 ug/mL for 15 minutes at 37°C and 5% CO_2. For T cell stimulation PBMCs were centrifuged at 500 xg for 5 minutes then re-suspended in 100 uL hR10 containing 1 ug/mL anti-human CD28/CD49d costimulatory cocktail (BD Biosciences), and either media (unstimulated) or 1 ug/mL SARS-CoV-2 Prot_S Complete Peptivator (Miltenyi). Cells were incubated for 24 h at 37°C and 5% CO_2. After 20 hours, cells were stained with anti-CD40L(CD154) BV605 (Biolegend, Clone 24-31). Also at this time, positive control wells were treated with 1x Cell Stimulation Mix (eBioscience) containing a cocktail of phorbol 12-myristate 13-acetate (PMA) and ionomycin. All cells were returned to the incubator for an additional 4 hours. After 24 hours total stimulation, cells from replicate wells were combined, centrifuged at 500 xg for 5 minutes, and blocked for 30 minutes at room temp in a 50 uL cocktail containing 5 uL Human TruStain FcX (Biolegend), 1 uL Ghost Dye Violet 510 (Tonbo), 1 uL $S_{167\text{-}180}$-tetramer-PE and 43 uL FACS buffer. Cells were then washed in FACS buffer and surface stained in 100 uL FACS buffer containing 5 uL each of anti-CD3 FITC (Biolegend, clone SK7), anti-CD200 PerCP/Cy5.5 (Biolegend, clone OX-104), anti-CD8 APC (Biolegend, clone SK1), anti-CD45RA BV421 (Biolegend, clone HI100), and anti-CD4 BV711 (Biolegend, clone OKT4) for 30 minutes at room temperature. Cells were washed twice in 200 uL FACS buffer, resuspended in 300 uL FACS buffer and analyzed by flow cytometry on a FACSAria II. Flow data were analysed in FlowJo. CD4+ AIM positive cells were defined as described in Painter et al. (2021), single live CD3+CD8-CD4+CD45RA-CD154+CD200+.

Monomer generation

HLA-DP4 monomers with the $S_{167\text{-}180}$ epitope were produced from purified HLA-DP4 containing the class II-associated invariant chain peptide (CLIP) (Niehrs et al., 2019) via HLA-DM catalyzed peptide exchange as described previously for HLA-DR (Scally et al., 2013). Briefly, HLA-DP4 CLIP was expressed in Trichoplusia Ni (Hi5) insect cells *via* a pFastBac-Dual construct encoding HLA-DPA1*01:03 α- and HLA-DPB1*04:01 β-chains with C-terminal fos/jun zipper domain. The HLA-DP4 β-chain further contained an N-terminal factor Xa cleavable CLIP sequence, and a C-terminal biotinylation signal and His_7 tag (Niehrs et al., 2019). Following expression for 3 days at 27 °C, cell supernatant was concentrated and buffer exchanged in a Tangential Flow Filtration system into 500 mM NaCl, 10 mM Tris-HCl pH8 and subsequently purified *via* immobilised metal affinity chromatography and Superdex S200 gel permeation chromatography (GPC) in 150 mM NaCl, 10 mM Tris-HCl pH8. The linked CLIP peptide was cleaved with factor Xa for 6 h at 21°C prior to peptide exchange, and factor Xa cleaved HLA-DP4 was subsequently incubated in the presence of a 10-fold molar excess of peptide and a 1/5 molar ratio of HLA-DM for 16h at 37°C in 100 mM sodium citrate pH 5.4. HLA-DP4 loaded with $S_{167\text{-}180}$ peptide was buffer exchanged into 50mM NaCl, 20 mM Tris-HCl pH8, purified via Hi-Trap Q ion exchange chromatography and biotinylated using BirA biotin ligase. Following a final Superdex S200 GPC step in PBS, biotinylated HLA-DP4-$S_{167\text{-}180}$ monomer was concentrated to approx. 1mg/ml and stored at -80 °C.

Tetramer generation and staining of Jurkat cells

Biotinylated HLA-DP4-monomers loaded with TFEYVSQPFLMDLE peptide ($S_{167\text{-}180}$) were tetramerized using PE-Streptavidin (Biolegend). One volume PE-conjugated streptavidin was added to one volume of HLA-DP4-monomer (1 mg/mL). The volume of

PE-streptavidin (0.2 mg/ml) was divided in 4 parts and added in 4 consecutive steps with 10 minutes incubation between. After adding all needed amounts of PE-streptavidin the mixture was incubated for at least 1 hour on ice prior to staining. Jurkat 76.7 cells expressing TCR4.1, TCR6.3, Jurkat 76.7 cell line expressing irrelevant TCR (specific to NQKLIANQF epitope from the spike protein of SARS-CoV-2 (Minervina et al., 2021b), and SARS-CoV-2 naive HLA-DPB1*04:01 positive donors' PBMCs were stained with 1 μL Ghost Dye Violet 510 Viability Dye (Tonbo Biosciences) and 1 μL of HLA-DPB1*04-$S_{167\text{-}180}$-tetramer. Cells were analyzed by flow cytometry on a custom-configured BD Fortessa using FACSDiva software (Becton Dickinson). Flow cytometry data were analyzed using FlowJo software (BD Biosciences). The quality of the $S_{167\text{-}180}$ HLA class II tetramer was judged by staining of the relevant T cell line and low background in irrelevant Jurkats and naive PBMCs.

Tetramer staining of SJTRC samples and scTCR sequencing

Donor PBMCs were thawed and resuspended in 100 μL FACS buffer (PBS, 0.5% BSA, 2 mM EDTA). Cells were stained with 5 μL Fc-block (Human TruStain FcX, Biolegend) and 1.5 μL of $S_{167\text{-}180}$ HLA class II PE-conjugated tetramer for 30 minutes on ice. After the incubation a cocktail of fluorescently-labeled surface antibodies (2 μL of each: Ghost Dye Violet 510 Viability Dye, Tonbo Biosciences; anti-human CD3 PerCP Cy5.5-conjugated, Biolegend, clone OKT3; anti-human CD4 BV711-conjugated, Biolegend, clone OKT4; anti-human CD45RA BV421-conjugated, Biolegend, clone HI100; and anti-human CCR7 FITC-conjugated, Biolegend, clone G043H7) was added. Samples were incubated for an additional 20 minutes on ice. Single, Live, CD3-positive, CD4-positive, tetramer-positive cells were sorted on the Sony SY3200 into 384-well plates with premixed SuperScript VILO cDNA Synthesis mix (Invitrogen) for subsequent scTCR sequencing. scTCR library preparation and sequencing was performed as previously described (Wang et al., 2012). In brief, cDNA underwent two rounds of nested multiplex PCR amplification with a forward primer mix specific for V-segments and reverse primers for C-segments of TCRalpha and TCRbeta and sequenced on Illumina MiSeq platform (2x150 read length). TCR sequences with undefined alpha-chain were excluded from the analysis. Resulting TCR sequences can be found in Table S2.

Bulk repertoire generation

TCRalpha and TCRbeta bulk repertoires were generated with the 5′RACE protocol described in (Egorov et al., 2015). RNA was isolated using Trizol reagent (Invitrogen) according to the manufacturer's protocol. All RNA was used for cDNA synthesis with SmartScribe kit (Takara), using template switch oligonucleotide and primers specific for TCRalpha and TCRbeta constant segments. cDNA was amplified in two rounds of PCR using Q5 high-fidelity polymerase (NEB). Adapters necessary for sequencing on the Illumina platform were introduced with the KAPA HyperPrep kit (Roche). Libraries were sequenced on Illumina MiSeq platform (2×150). Sample cell counts along with sequencing quality metrics are listed in Table S3.

Public TCR repertoire datasets

TCRbeta dataset for MIRA class II peptide stimulation (ImmuneCODE MIRA release 002.1) was accessed via ImmuneACCESS database (Nolan et al., 2020). Processed single cell paired chain TCR datasets from ARTE assays after 6 and 24 hour stimulation with SARS-CoV-2 peptides were used as supplied by authors in original publications: Table S3 from (Bacher et al., 2020) and Table S4A from (Meckiff et al., 2020).

QUANTIFICATION AND STATISTICAL ANALYSIS

TCR repertoire analysis

Bulk TCR repertoire data was demultiplexed and assembled into the UMI consensuses with *migec* (v. 1.2.7; with collision filter and force-overseq parameters set to 1) (Shugay et al., 2014). V and J-segment alignment, CDR3 identification and assembly of reads into clonotypes were performed with MiXCR (v. 3.0.3) with default parameters (Bolotin et al., 2015). Resulting processed repertoire datasets and reference to raw TCR repertoire sequencing data are available at GEO database (acc. GSE183393). Analysis of bulk repertoire data was performed using R language for statistical computing, with merging and subsetting of data performed using *data.table* package. *stringdist* and *igraph* R packages were used to build TCR similarity network, *gephi* software was used for TCR similarity networks layout and visualization and *ggplot2* library for other visualizations.

Statistical analysis

Descriptive and comparative statistics were employed in the manuscript as described in the figure legends with the number of replicates indicated.

Supplemental figures

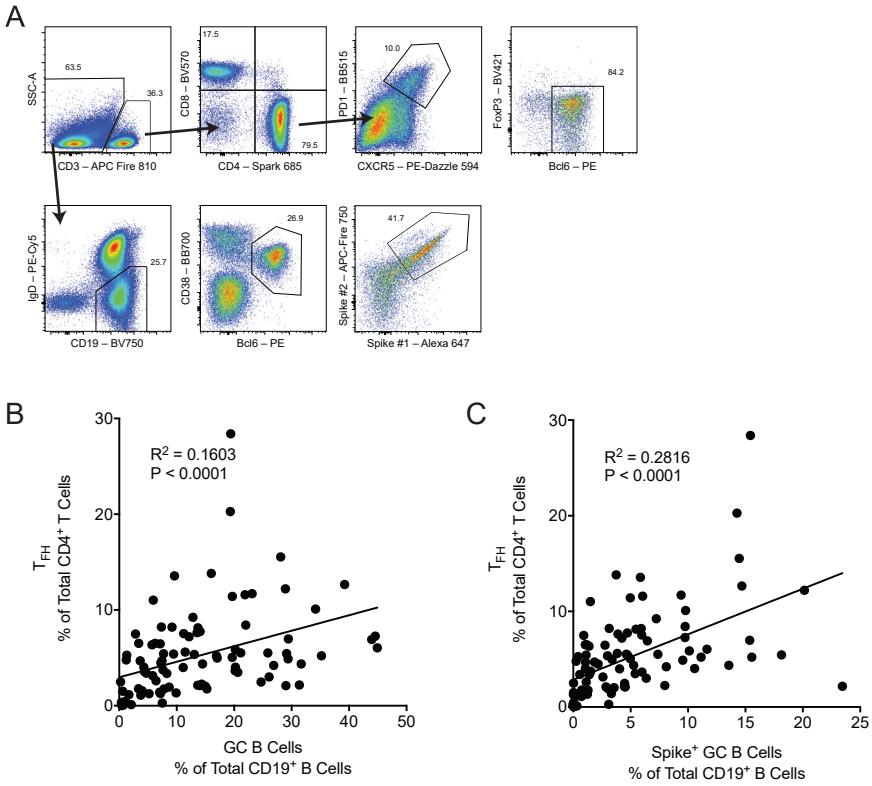

Figure S1. Human lymph node T_{FH} population frequency correlates with the GC B cell population frequency, related to Figure 1; Tables 1 and S1

(A) Gating strategy for the lymph node T_{FH} ($CD3^+CD4^+CXCR5^+PD1^+Bcl\text{-}6^+FoxP3^-$) and GC B cell ($CD19^+IgD^{low}Bcl\text{-}6^+CD38^{int}$) populations. $Spike^+$ GC B cells are gated on cells that stain positive for two individual SARS-CoV-2 spike-protein probes.

(B) The T_{FH} population measured as the frequency of total lymph node $CD4^+$ T cells were compared with the total frequency of lymph node GC B cells using linear regression.

(C) Total T_{FH} population frequency compared with the total frequency of spike-specific GC B cells. n = 95 individual lymph node samples obtained from all 15 study subjects between and including study days 21 and 200.

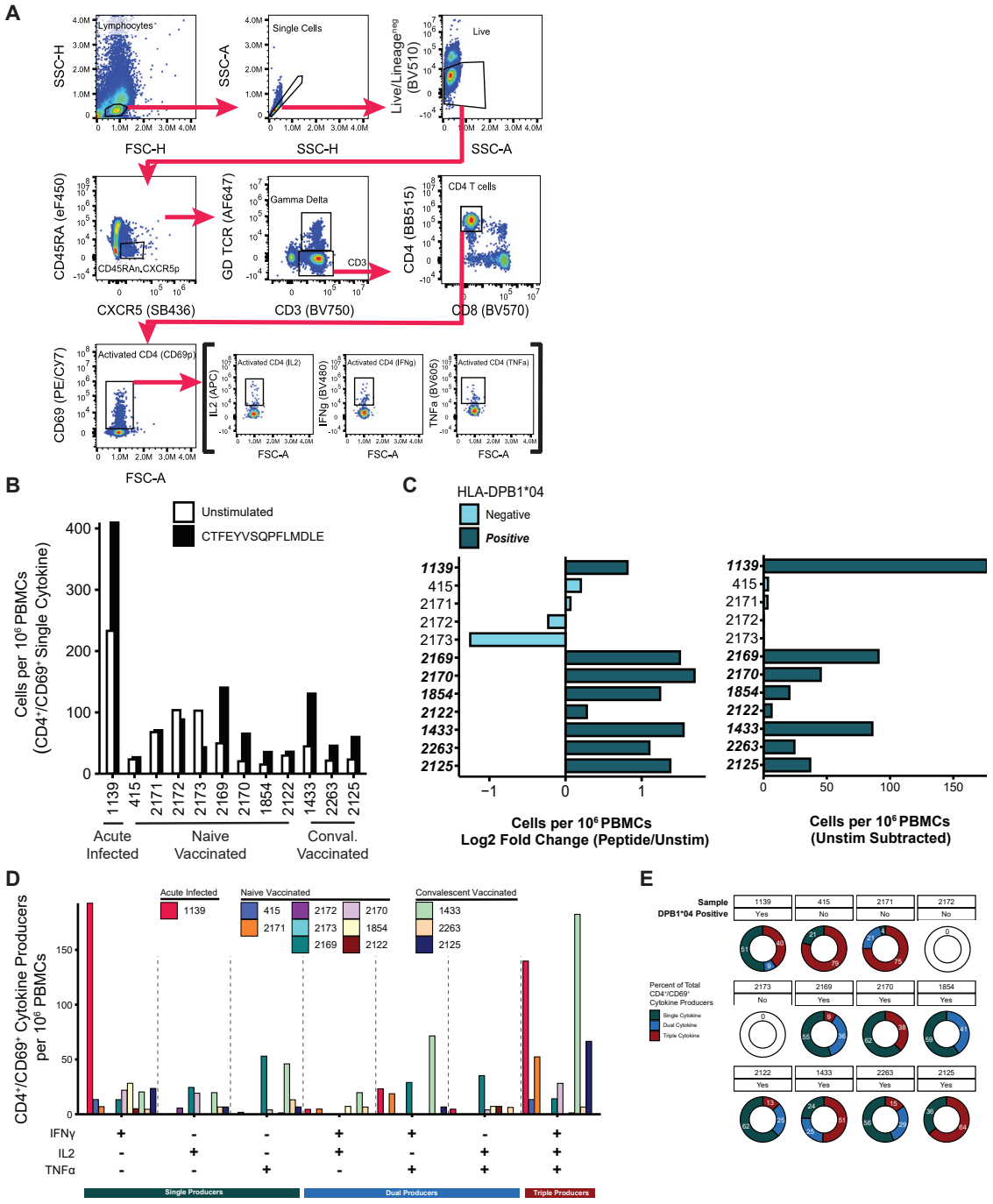

Figure S2. Intracellular cytokine staining of PBMCs stimulated with $S_{166–180}$ peptide, related to Figure 2C

(A) Gating strategy employed to resolve $CD4^+/CD69^+$ T cells producing IL2, TNFα, or IFNγ. Activated $CD4^+$ T cells were defined as live/B cell lineage $(CD19^+)^{neg}$/T_{FH} lineage $(CD45RA^-/CXCR5^+)^{neg}/\gamma\delta$ TCR^{neg}/ $CD3^+/CD4^+/CD69^+$ and Boolean gated on $IL2^+$, $TNF\alpha^+$, or $IFN\gamma^+$ single-positive lymphocytes.

(B) The number of $CD4^+/CD69^+$ T cells producing IL2, TNFα, or IFNγ per 10^6 PBMCs following CTFEYVSQPFLMDLE peptide (black) or media (white) stimulation.

(C) $CD4^+/CD69^+$ T cells producing IL2, TNFα, or IFNγ per 10^6 PBMCs from DPB1*04:01/02-positive (dark teal bars; bold-italicized Sample ID) and -negative (light blue bars) participants presented as the Log_2 fold change of peptide-stimulated over unstimulated (left) and after background subtraction of unstimulated (right).

(D) The number of $CD4^+/CD69^+$ T cells (unstimulated portion subtracted) producing combinations of IL2, TNFα, and/or IFNγ per 10^6 PBMCs.

(E) Percentage of single, dual, and triple cytokine-producing $CD4^+/CD69^+$ T cells among total cytokine-producing $CD4^+/CD69^+$ T cells. Values calculated from cells per 10^6 PBMCs after background (unstimulated) subtraction. Differential Boolean gating on IFNγ, IL2, and TNFα was used to distinguish cytokine-producers; values in (D; color-coded bars at bottom) comprise the percentages in (E).

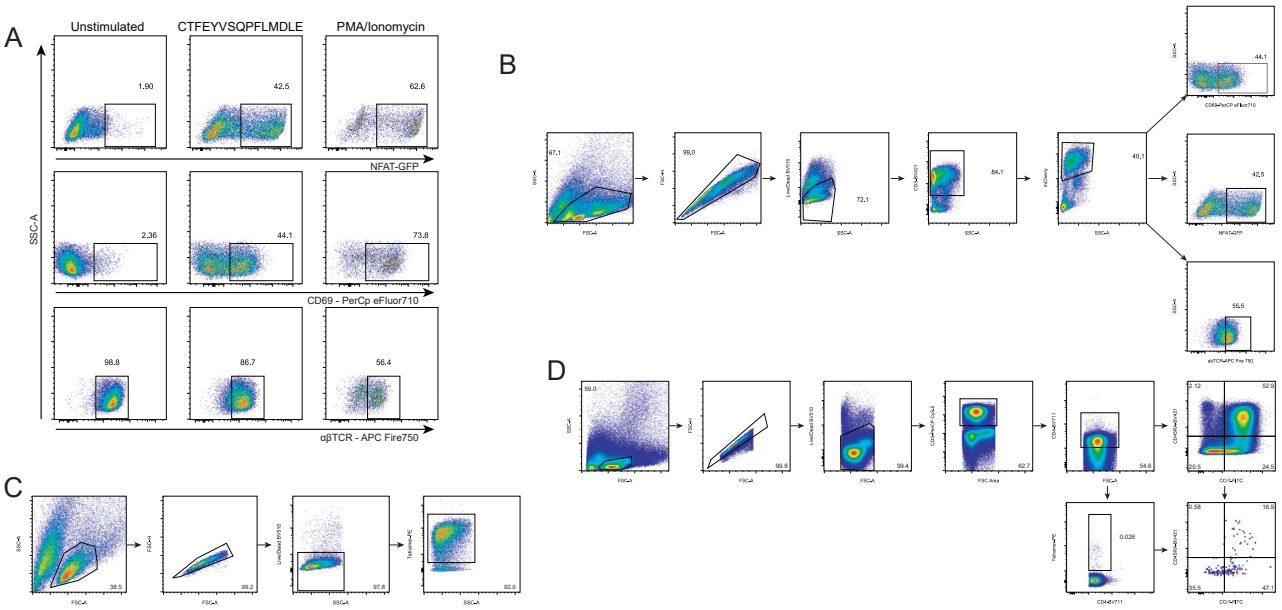

Figure S3. $S_{167–180}$ epitope discovery and validation, related to Figure 2

(A) Jurkat cell line expressing the predicted TCR after stimulation with the predicted epitope. Left column: negative control; middle column: TCR6.3 cell line co-cultured with PBMCs from healthy DPB1*04:01-positive donor pulsed with CTFEYVSQPFLMDLE peptide ($S_{166–180}$); right column: positive control. Top row: NFAT-GFP reporter expression. Middle row: CD69 surface expression. Bottom row: downregulation of the TCR on cell surface.

(B) Gating strategy for (A), Figures 2D and S4.

(C) Gating strategy for Figure 2E.

(D) Gating strategy for Figure 2F.

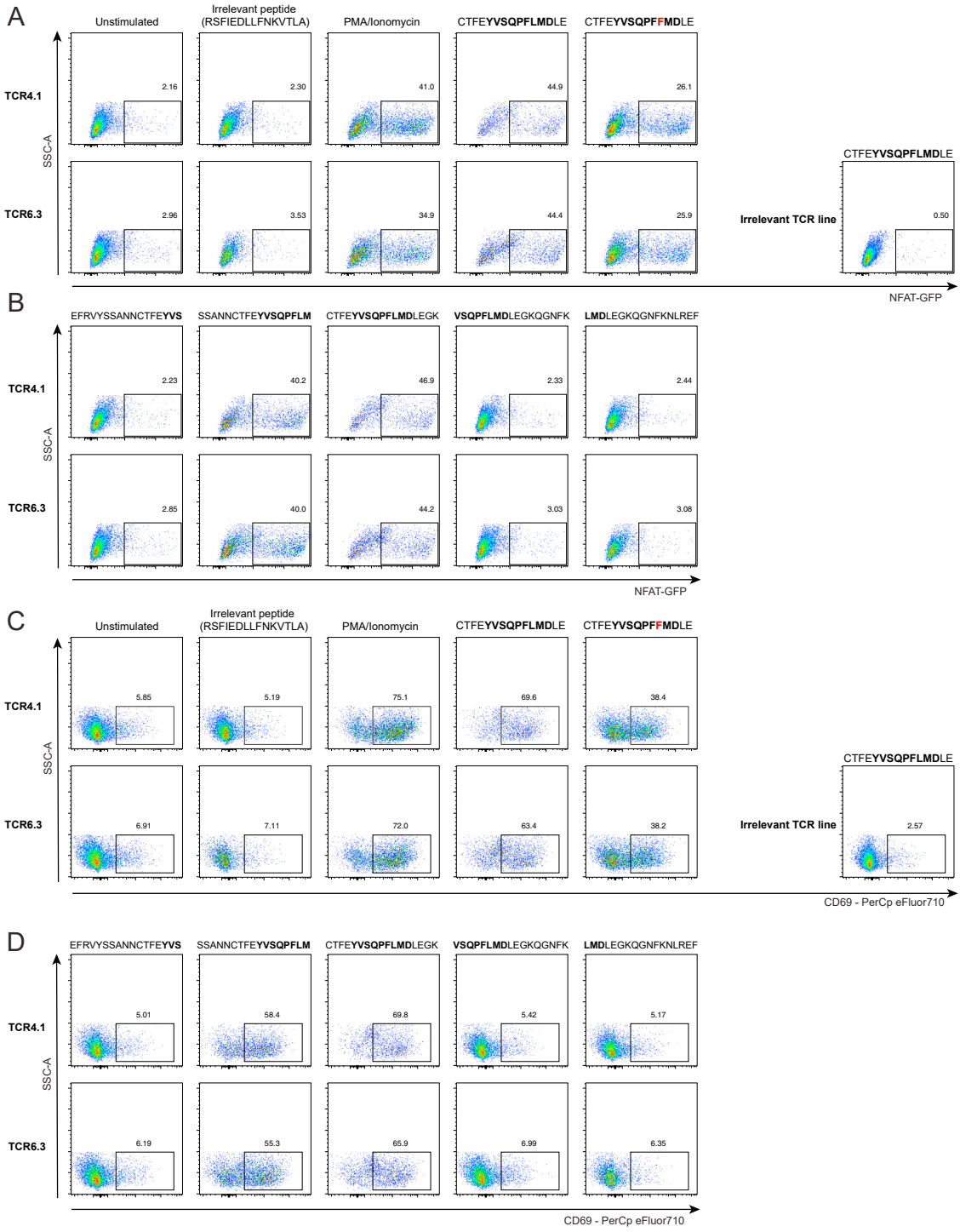

Figure S4. Peptide stimulation of Jurkat cell lines expressing the predicted $S_{167–180}$ specific TCRs, related to Figure 2

(A and B) NFAT-GFP reporter expression.

(C and D) CD69 surface expression. Incubation without peptide (unstimulated) and with irrelevant SARS-CoV-2 derived DPB1*04-restricted peptide (RSFIEDLLFNKVTLA described in Dykema et al. 2021 and Loyal et al. 2021) as well as stimulation of line expressing irrelevant TCR (specific to NQKLIANQF epitope from the spike protein of SARS-CoV-2, described in (Minervina et al., 2021b) with CTFEYVSQPFLMDLE peptide were used as negative controls.

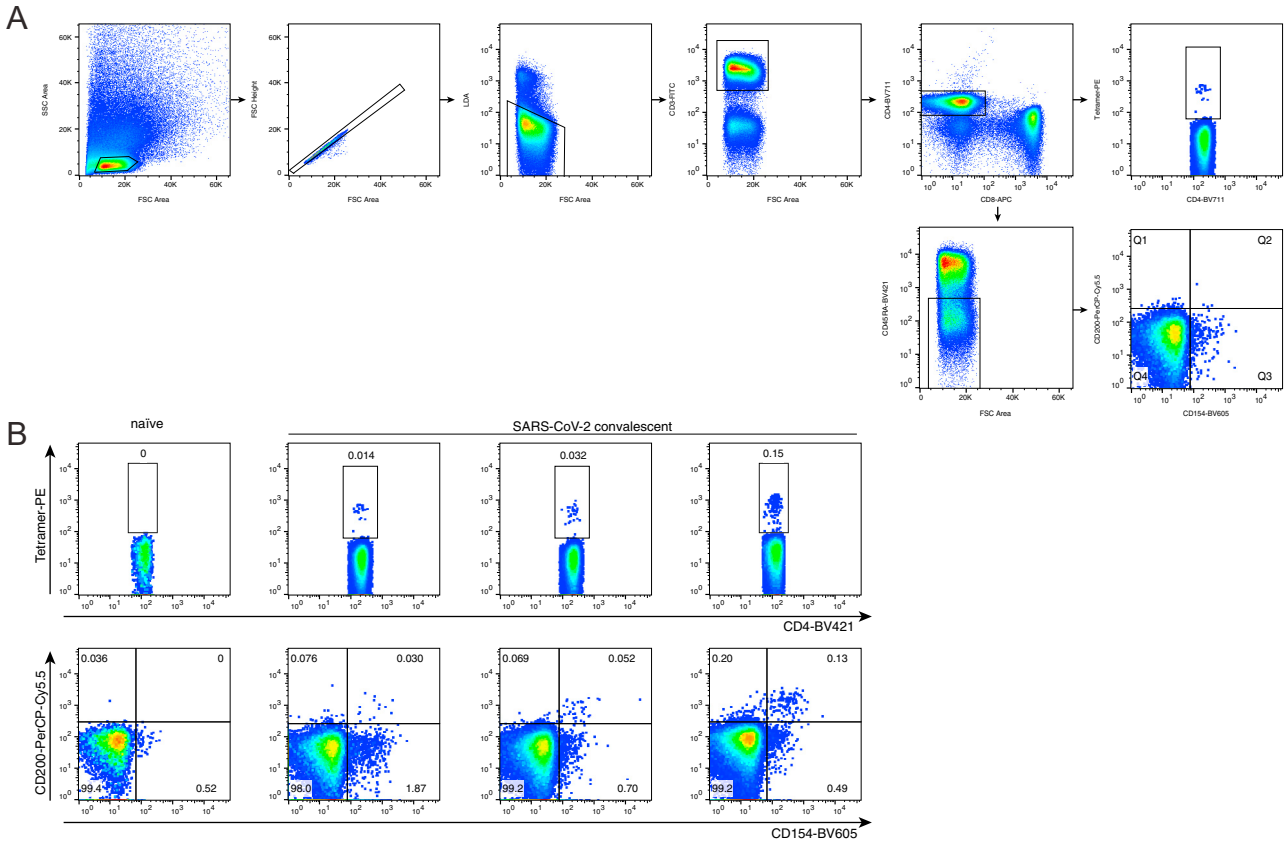

Figure S5. Frequency of $S_{167–180}$ tetramer$^+$ cells in comparison to the frequency of total spike AIM$^+$ cells, related to Figure 2

(A) Gating strategy. Tetramer-positive cells were gated as cell-sized single live CD3$^+$CD4$^+$tetramer$^+$, AIM$^+$ cells were defined as cell-sized single live CD3$^+$CD4$^+$CD45RA$^-$CD154$^+$CD200$^+$.

(B). $S_{167–180}$ tetramer$^+$ cells (top row) and AIM$^+$ (bottom row) for SARS-CoV-2 naive donor (left column) and SARS-CoV-2 convalescent donors.

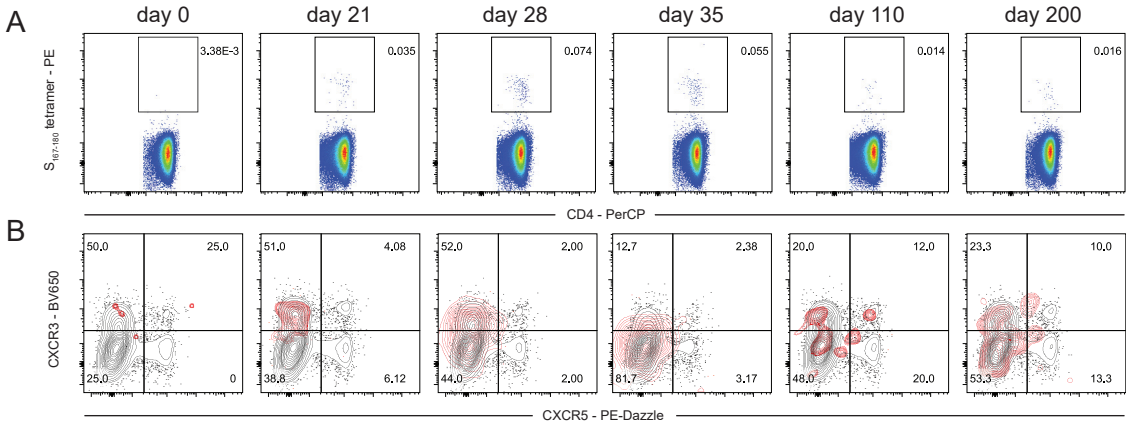

Figure S6. $S_{167–180}$-specific $CD4^+$ T cell response in peripheral blood of subject 16 following BNT162b2 vaccination is principally biased toward CXCR3 and not CXCR5 expression, related to Figure 3

(A) $S_{167–180}^+$ $CD4^+$ T cell responses over time in subject #16.

(B) CXCR3 and CXCR5 surface expression on tetramer-positive cells (red) and total $CD4^+$ T cells (black) are visualized with overlaid contour plots. Provided frequencies are the frequency of $S_{167–180}$-tetramer-positive cells in the indicated quadrant.